Untersuchung des mechanischen Verhaltens von kompaktiertem Salzgrus im Kontakt mit dem Wirtsgestein

Ergebnisbericht zum
BMBF-Forschungsvorhaben
02 E 9904

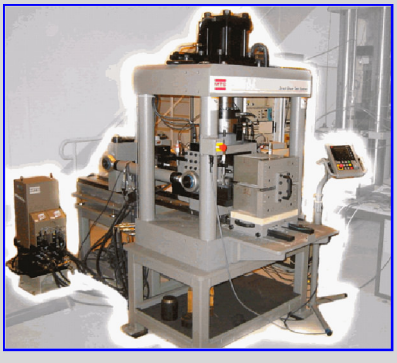

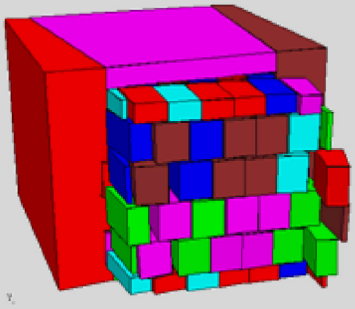

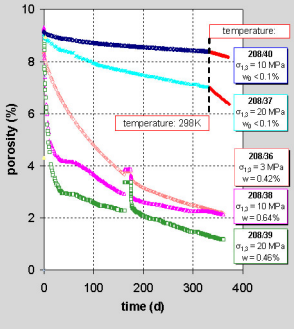

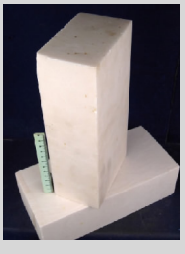

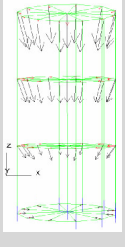

Institut
für
Gebirgsmechanik
GmbH

Kurzfassung

Im Salzkonzept für die Endlagerung hoch-radioaktiver Abfälle in tiefen geologischen Formationen ist Salzgrus aufgrund seiner günstigen Eigenschaften das bevorzugte Material von verbleibenden Hohlräumen. Allerdings ist die anfängliche hydraulische Dichtwirkung derartiger Verfüllmassen infolge ihrer hohen Anfangsporosität eingeschränkt. Neben verschiedenen anderen Ansätzen bildet die Verwendung von vorkompaktierten Formsteinen eine erfolgversprechende Alternative für Verschlußkonzepte.

Die vorgestellten Untersuchungen wurden sowohl von der Europäischen Kommission im Rahmen des internationalen 6. EU-Rahmenprogramms (2002 - 2006) als auch vom Bundesministerium für Bildung und Forschung (BMBF) unter dem Förderkennzeichen 02 E 9904 gefördert.

Die hier durchgeführten Untersuchungen umfassen die Charakterisierung des mechanischen Kompaktionsverhaltens in Kopplung mit der davon abhängigen Entwicklung der Transporteigenschaften von sogen. Salzziegeln (kaltgepresster Salzgrus mit einer Porosität von ca. 8%), sowie deren Kontaktflächenverhalten untereinander bzw. zum Gebirge. Sie sind die Vorrausetzung für die Entwicklung von Stoffgesetzen zur Beschreibung des Kompaktionsverhaltens in der Niedrig-Porositätsregion (10% - 1%), sowie, darauf aufbauend, der Eigenschaften der Kontaktflächen. Eine Schlüsselfunktion ist dabei das Verständnis des Einflusses von Wasser, weil es in komplexer Weise die gekoppelten hydraulisch/mechanischen Eigenschaften von Steinsalz beeinflusst. Die Untersuchungen umfassen die folgenden Schwerpunkte:

(1) Triaxiale Kompressions- und Permeabilitätstests bei unterschiedlichen Manteldrücken.

(2) Gasinjektionstests an lösungsgesättigten Proben zur Bestimmung von 2-Phaseneffekten (z.B. Gaseindringdruck).

(3) Langzeitkompaktionstests unter hydrostatischer Einspannung mit bzw. ohne Zugabe von Salzlösungen.

(4) Direkte Schertests zwischen Salzziegeln bzw. im Kontakt zum Gebirge mit Befeuchtung bzw. ohne.

(5) Anpassung und Überprüfung von Stoffgesetzen für das Kompaktions- und Kontaktflächenverhalten.

EUROPEAN COMMISSION

Community Research

NF-PRO

(Contract Number: F16W-CT-2003-02389)

WP 3.5

- Crushed Salt Engineered Barrier Behaviour -

Investigation of the Mechanical Behaviour of Pre-compacted Crushed Salt in Contact to the Host Rock

Final Activity Report

Deliverable 3.5.6b

Author(s): Klaus Salzer, Till Popp, Heinz Böhnel,
Dirk Naumann and Jan Mühlbauer (IfG)

Reporting period: 01/01/05 – 15/12/07

Date of issue of this report: **15/11/07**

Start date of project: **01/01/04** Duration: 48 Months

DISTRIBUTION LIST

Project co-funded by the European Commission under the Euratom Research and Training Programme on Nuclear Energy within the Sixth Framework Programme (2002-2006)		
Dissemination Level		
PU	Public	
RE	Restricted to a group specified by the partners of the NF-PRO	
CO	Confidential, only for partners of the NF-PRO project	

Name	Number of copies	Comments

Table of Contents

1 INTRODUCTION 4

2 EXPERIMENTAL CONDITIONS 7

2.1 SAMPLE CHARACTERISTICS AND PREPARATION 7
2.2 ROCK MECHANICAL PROCEDURES 8

3 LABORATORY INVESTIGATIONS 10

3.1 STRENGTH AND CREEP PROPERTIES OF DRY MATERIAL 10
3.2 LONG TERM CREEP TESTS ON WET AND DRY SAMPLES 12
3.3 PERMEABILITY TESTS ON DRY SAMPLES 15
3.4 CAPILLARY THRESHOLD EFFECTS IN A WET SAMPLE 17
3.5 SHEAR-TESTS BETWEEN DRY OR WET SALT-BRICK SURFACES 21

4 CRUSHED SALT CONSTITUTIVE MODELS 24

4.1 MATERIAL LAW SELECTION 24
4.2 ITASCA CRUSHED-SALT CONSTITUTIVE LAW 24
4.3 HEIN CONSTITUTIVE LAW 24
4.4 ZHANG CONSTITUTIVE LAW 24
4.5 SPIERS CONSTITUTIVE LAW 24

5 MECHANICAL CONTACT PLANE PROPERTIES BETWEEN SALT-BRICKS 24

5.1 INTRODUCTION 24
5.2 THE MINKLEY-SHEAR MODEL 24
5.3 APPLICATION TO THE MINKLEY-SHEAR MODEL AND RECALCULATION 24

6 SUMMARY AND CONCLUSION 24

LITERATURE 24

Deliverable 3.5.7:

- **Final report**

Authors: Klaus Salzer, Till Popp, Heinz Böhnel, Dirk Naumann and Jan Mühlbauer

(Institut für Gebirgsmechanik GmbH, Leipzig – IfG)

The studies presented in this report have been funded as part of the integrated project NF-PRO jointly by the European Commission under the Euratom Research and Training Programme on Nuclear Energy within the Sixth Framework Programme (2002-2006), and the German Federal Ministry of Research and Education under contract 02 E 9904.

1 Introduction

The storage of radioactive waste in deep geological rock formations is the only accepted alternative for a save long-term disposal to exclude a threat to actual and future generations. To ensure containment and long-term retardation of radionuclide releases various storage concepts for radioactive waste have been developed based on a complex system of geological and technical barriers (so-called multi-barrier system). Besides clay and crystalline rock formations salt deposits are internationally evaluated as host rocks, e.g. by the USA, the Netherlands and Germany.

Backfill and seals are an important part of the technical, better called as "engineered barrier system" (EBS) which represents the man-made, engineered materials placed within a repository, in addition to the waste form, waste canisters. The EBS and those parts of the host rock in contact with or near the EBS, whose properties have been affected by the presence of the repository belong to the so-called "near-field". The "far-field" represents the geosphere (and biosphere) beyond the near-field.

Due to its importance for the repository safety performance, the understanding of the backfill behaviour in the repository is an important prerequisite for repository design and construction and repository performance assessment.

In the salt concept crushed salt was selected as the most suitable backfill material because

(1) it has good compacting properties,
(2) its thermal and mechanical properties are similar to the surrounding rock salt (after reconsolidation, see below) and
(3) it is easy available.

During the time-dependent closure of drifts and boreholes caused by thermo-mechanical creep of the surrounding salt rock the crushed salt will be compacted and its initial porosity

and permeability will decrease as demonstrated in large scale in situ-experiments, e.g. in the Amelie mine (Kazan & Ghoreychi 1996) and the Asse salt mine (Bechthold et al. 1999, 2004). Over long time periods, the crushed salt is expected to gradually reconsolidate into a material comparable to virgin rock salt.

However, a limiting factor for the use of saliferous granulates as backfill is their initially high porosity and permeability, resulting in a low sealing capacity and mechanical integrity just after emplacement. Besides adding bentonite to enhance compaction and to reduce permeability, an alternative concept for sealing is the use of pre-compacted salt elements, e.g. bricks, which are characterized by porosities below 10% resp. low permeability and high uniaxial strength (Stockmann 1994).

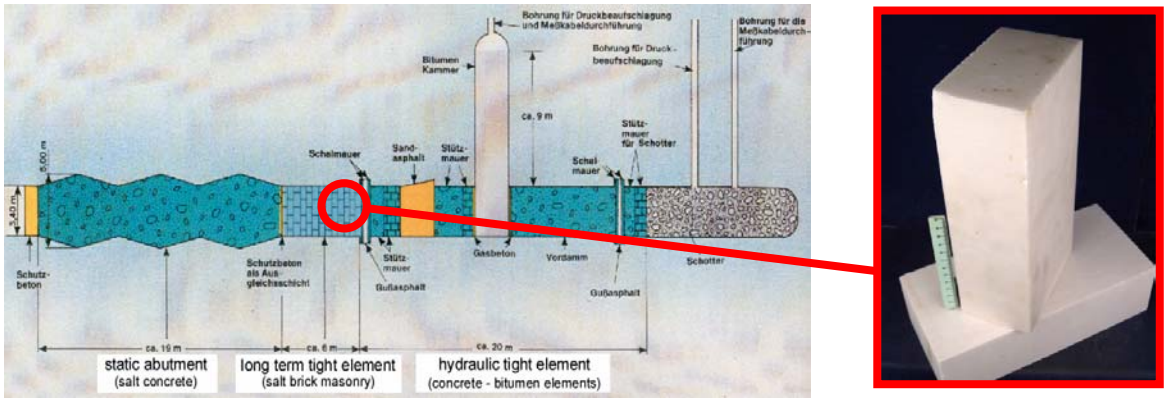

Figure 1-1. The long term tight element in the Asse dam project to built up by salt bricks of higly pre-compacted crushed salt (after Stockmann 1994).

Depending on whether granular salt or pre-compacted salt bricks are used reliable descriptions of both, the mechanical long term behavior and fluid transport properties of both salt and backfill system, are therefore of urgent need for final performance assessment. Whereas the creep (e.g. Hunsche & Schulze 1994; Spiers & Carter 1998) and transport behavior of natural rock salt (e.g. Stormont & Daemon 1992; Popp et al. 2001; Popp et al., 2007) and of crushed rock salt with porosities above 10-15% (e.g. Bechthold et al. 2004) have been thoroughly studied only limited knowledge exists regarding the processes that convert permeable salt backfill materials (porosity <10%) into an impermeable backfill with properties similar to those of natural salt rock. Furthermore, there is a fundamental demand in research and development regarding the understanding and adequate description of the mechanical behaviour of the contact between the highly compacted granular salt and the host rock as well as

between blocks made of highly compacted granular salt among themselves and the host rock.

Our laboratory investigations are aiming at a comprehensive data basis regarding compaction and hydraulical behavior of the pre-compacted salt bricks (initial porosity <10%) with respect to the numerical description of their long-term behavior if they are used as sealing elements. Special account is given to humidity effects, affecting both, mechanical and hydraulical properties. The investigations are focusing on the following issues:

(1) Triaxial compression and permeability tests at different confining pressures on highly precompacted crushed salt samples.
(2) Gas injection tests on fluid saturated salt bricks with respect to 2-phase properties (e.g. permeability and threshold pressure).
(3) Long term hydrostatic compaction tests with and without added brine, respectively.
(4) Shear-tests at increasing normal pressure between highly pre-compacted crushed salt blocks and host rock (rock salt) including wetting with brine.

The performed laboratory tests were already comprehensive reported in three deliverables focusing on the following issues:

(1) Triaxial compression and permeability tests at different confining pressures on highly pre-compacted crushed salt samples including brine injection (IfG, 2005: **Deliverable 3.5.3**).
(2) Shear-test at increasing normal pressures between highly pre-compacted crushed salt blocks including brine injection and shear-test at increasing normal pressures between highly pre-compacted crushed salt blocks and host rock (rock salt) including brine injection (IfG, 2005: **Deliverable 3.5.4**).
(3) Report on long-term creep tests and gas injection tests on moistened salt bricks during compaction (IfG, 2006: **Deliverable 3.5.5**).

On the basis of these experimental results two theoretical studies for adaptation appropriate material laws could be realized and were reported in detail in the following deliverables:

(4) Report an adaptation of material laws to laboratory results ((IfG, 2006: **Deliverable 3.5.6**).
(5) Report an adaptation of material laws to laboratory results – shear test and shear model (IfG, 2006: **Deliverable 3.5.6a**).

Preliminary results of the performed experimental work were presented by SPIERS (Univ. Utrecht) at the 2nd workshop in Cardiff (GB) (10/19/2005 – 10/21/2005). In addition, interims results were presented as posters by Salzer et al. at the 3rd NF-PRO workshop in San Lorenzo de El Escorial (E) (11/14/2006 – 11/16/2006) and by Salzer et al. at the 4th NF-PRO workshop in Brussels (Be) (10/15/2007 – 10/17/2007).

Salzer, K., T. Popp & H. Böhnel (2006/2007): Mechanical and permeability properties of highly pre-compacted granular salt bricks. (Posters).

In addition, a summary of the experimental work is published by Salzer et al. (2007) in the Proc. of the Sixth Conf. on the Mech. Behavior of Salt. held in Hannover in May 2007:

Salzer, K., T. Popp & H. Böhnel, (2007): Mechanical and permeability properties of highly precompacted granular salt bricks. In K.-H. Lux, W. Minkley, M. Wallner, & H.R. Hardy, Jr. (eds.), Basic and Applied Salt Mechanics; Proc. of the Sixth Conf. on the Mech. Behavior of Salt. Hannover 2007. Lisse: Francis & Taylor (Balkema). 239 – 248.

The objective of the final report is to summarize the now existing comprehensive experimental database and the results of adaptation studies of material laws to laboratory results as well for the material behaviour of the precompacted crused salt bricks as for the mechanical parameters of contact planes between bricks of crushed rock salt and, as well the contact between such bricks and the natural host rock, i.e. rock salt.

2 Experimental conditions

2.1 Sample characteristics and preparation

A salt brick used in our investigations is a cold pressed (p ≥130 MPa in some few seconds) artificial rectangular solid (240 mm x 115 mm x 71 mm; ±1%) of highly compacted crushed salt composed of nearly pure sodium chloride (≥ 95% NaCl) with grain sizes between <0.16 mm and 0.5 mm. Such specimens of salt bricks have been produced in large series by the company K+S in 1990 in advance of the planned in situ test dam construction in the Asse salt mine. The fabrication of the salt bricks is already described in detail in Stockmann (1994). A summary of their petrophysical properties is given in Table 2-1.

Cylindrical test specimen were drilled from a salt brick and then trimmed with a turning lathe to its final dimensions (depending on the test type). The masses of the samples were qualified with a precision balance (± 0.01 g) and their dimension (diameter and height) were measured with a digital sliding caliper (± 0.1 mm). The specimen density is calculated from the weight and volume of the test sample.

Impregnation of so called ‘wet’ samples was performed with saturated NaCl-brine (density: ρ = 1.205 g/cm³ at 21°C; source: Asse-mine, Germany) storing them in a brine filled container which was evacuated for 5 minutes up to 1 mbar. It has to be mentioned that despite the always equal procedure the amount of brine absorbed by the various specimens is different and significantly lower than it was estimated on the basis of the initial porosity of around

8%. There is only a correlative dependency between the porosity/density and the absorbed volume of brine, which varies between 0.85 and 1.3 Vol.-%. Therefore, it can be concluded that only a partial pore space is accessible for brine and most of pore space is composed of isolated pores.

Table 2-1. Standard salt brick properties for the use in dam buildings (Salzer et al., 1999)

Parameter	Value	Investigation technique
Dimensions	240 x 115 x 71 mm (± 1%)	
Density[*)]	1950 kg/m^3 (± 1%)	DIN 18 125 T1
Porosity[*)]	9 % ±1%	
H_2O-content[*)]	0.2 % (± 10%)	DIN 18 121 T1
Vp	4.13 ±0.02 km/s	
Vs	2.35 ±0.01 km/s	
Shear modulus[*)]	11 ±0.1 GPa	DIN 18 137 T1
Young's modulus[*)]	27.75 ±0.22 GPa	compare DGEG
Uni-axial strength[*)]	59.8 ±1 MPa	compare DGEG
Bulk modulus[*)]	19.35 ±0.21 GPa	compare DGEG

DGEG: Empfehlungen Nr. I, 2,16,17 des AK "Felsmechanik" der DGEG e.V. - Zeitschrift Bautechnik 56, 71.

[*)] Tested on sample cylinders with 144 mm length and 70 mm diameter (Salzer et al., 1999).

[**)] Taken from Stockmann et al, 1994.

2.2 Rock mechanical procedures

The strength testing experiments were performed in a standard Karman-cell in the servo-hydraulic testing machine (RBA 2500, Schenk/Trebel Germany). The cylindrical samples (144 mm height and 72 mm diameter) are sealed with rubber tubes and oil is used as confining medium. Outside the vessel three LVDT transducers are mounted between the piston and the load frame near the sample for the measurement of the axial strain. The axial load is determined from an external load cell. Deformation induced volume changes ΔV of the specimens are determined by a volume balance of the oil volume changes as measured via the pressure intensifier and the axial piston displacement in the cell.

During the tests permeability can be measured simultaneously parallel to the sample cylinder axis using the stationary flow method (e.g. Popp et al., 2001). To maintain access of the gas to the sample, a central hole exists in the pistons whereby the specimens are additionally

prepared with small boreholes on their axial ends (diameter 5 mm, length 35 mm) to minimize end effects during straining.

Triaxial creep tests at constant deviatoric stresses and compaction tests at quasi-hydrostatic conditions respectively were performed on smaller specimens (80 mm height and 40 mm diameter) in a creep-test rig equipped with Karman-cells. The axial stress comes from a mechanical load device, which can be used in a range up to 200 kN, while the confining pressure (up to 30 MPa) results from a hydraulic system kept constant by an accumulator. The axial load is determined by a calibrated load cell before each experiment. Axial stress and confining pressure are kept constant with an accuracy of ±1% during the tests. All test parameters like axial deformation (three dial gauges), confining pressure and temperature were manually checked and recorded daily.

Figure 2-1. Direct shear system (MTS model 816) in the lab of the IfG Leipzig.

To determine the contact properties between the salt bricks itself and the salt contour, we used the shear testing equipment (MTS Systems Corporation model 816) installed at the IfG (Figure 2-1). As main advantage, it allows new types of testing procedures for direct shear tests with different boundary conditions (for experimental details see Blümel, 2000).

3 Laboratory investigations

3.1 Strength and creep properties of dry material

In advance of the usage of salt bricks as a dry masonry abutment for a dam construction various specimens were tested regarding their strength behaviour. Stress-deformation curves (in strain control) were recorded for a constant deformation rate of $\dot{\varepsilon}_1 = 2.5 \cdot 10^{-5}\ s^{-1}$ at room temperature (23°C). Constant confining pressures were applied in stages of σ_3 = 0, 2, 5, 10 and 20 MPa.

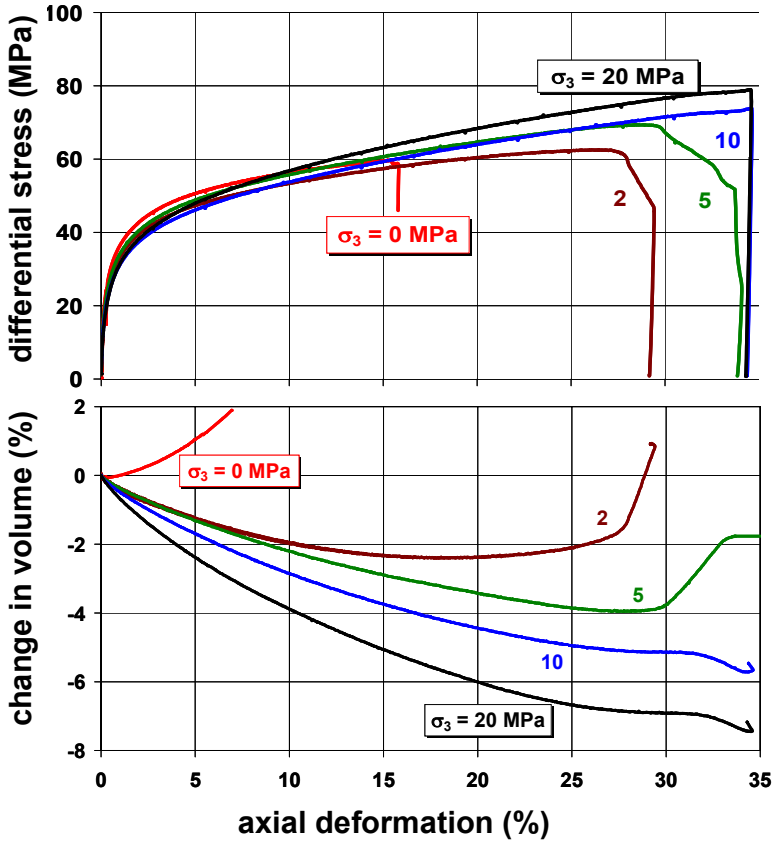

Figure 3-1. Summary of triaxial strength tests on salt bricks at 23°C. (above) stress-strain curves, (below) dilatancy as a function of axial strain.

As summarized in Figure 3-1, the stress-strain curves exhibit strain hardening in the pre-failure range, whereas the evolution of dilatancy occurs only at uniaxial stress resp. at higher axial deformation. The dominating effect of sample compaction, in accordance to confining pressure, is still visible. Due to the sample compaction it has to be mentioned that the axial stresses need to be corrected referred to the actual sample diameter. However, although

such a correction can be done based on the relationship between measured axial and volumetric strains only the non-corrected values are shown in a conservative manner in Figure 3-1.

Remarkably, the load bearing capacity and dilatancy behaviour of the crushed rock salt test specimens differ from the behaviour of the compact natural rock salt due to reachable larger deformations, relatively high load bearing capacities and the reduction of the dilatancy due to the decrease of pore space. Most important, dilatant deformation resp. shear failures occur only in a low peripheral pressure range ($\sigma_3 \leq 5$ MPa). At higher pressures ($\sigma_3 \geq 10$ MPa) no failure is observed. The general deformation style corresponds to the macroscopic appearance of deformed specimens (Figure 3-2).

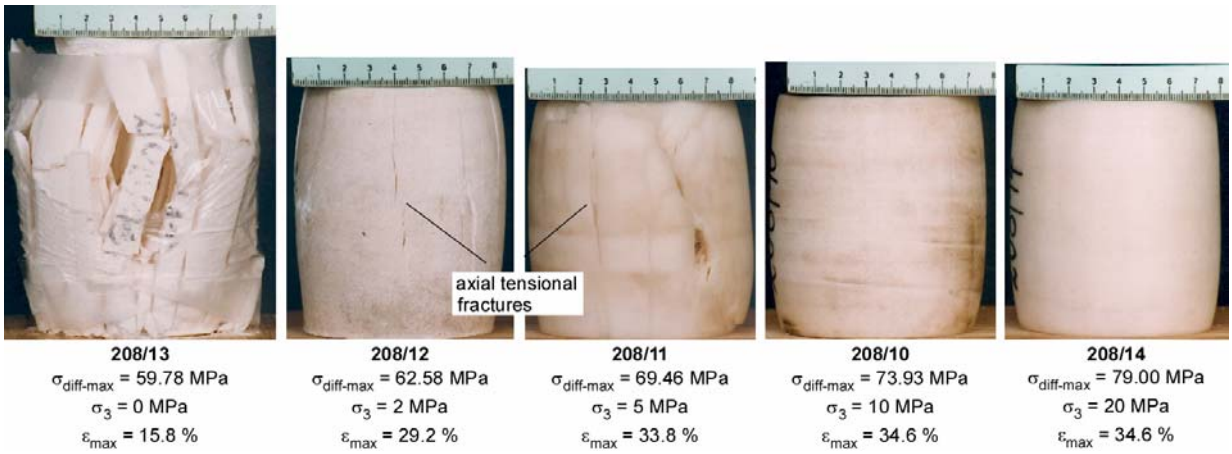

Figure 3-2. Axially deformed cylindrical salt bricks specimens after testing at various confining pressures and at constant strain rate of $2.5 \cdot 10^{-5}$ 1/s. Note the change of the deformation style from brittle to ductile due to the increasing confining pressure.

However, it is important that the strength of the salt bricks is drastically reduced if brine is present. Although this effect was not systematically investigated, one experiment performed with a wet sample (at σ_3 = 10 MPa) showed a systematically lowered strength behaviour (around 15 MPa) compared to the reference sample at dry conditions.

As a supplementary test, specimen 27 was compressed with a lateral to vertical stress ratio of $\sigma_3 = 0.33 \cdot \sigma_1$ aiming on a nearly constant cross section during axial deformation (with $\Delta\varepsilon_V \approx \Delta\varepsilon_1$) corresponding to a quasi-oedometer test. However, the test showed, that a factor of 0.33

is too small to avoid bulging of the test specimen (compare Table 3-2). Probably the ratio is in the order of $\sigma_3 \approx 0.4 \cdot \sigma_1$.

3.2 Long term creep tests on wet and dry samples

With respect to long-term properties laboratory creep tests on cylindrical salt brick samples (l = 80 mm, d = 40 mm) were carried out to validate the material parameters used for modelling. An evaluation of the creep rates after the NORTON's law (e.g. Hunsche and Schulze 1994)

$$\dot{\varepsilon}_{Krs} = K \cdot (\sigma_1 - \sigma_3)^n \qquad (3\text{-}1)$$

gives the relatively low stress exponent n = 2.93. This implies that besides dislocation glide/creep in the halite crystals further mechanisms contribute to the overall deformations. Presumptively, solution-precipitation creep or "pressure solution" (e.g. Spiers & Carter 1998, Bechthold et al 2004) plays an important role as a quasi-viscose part.

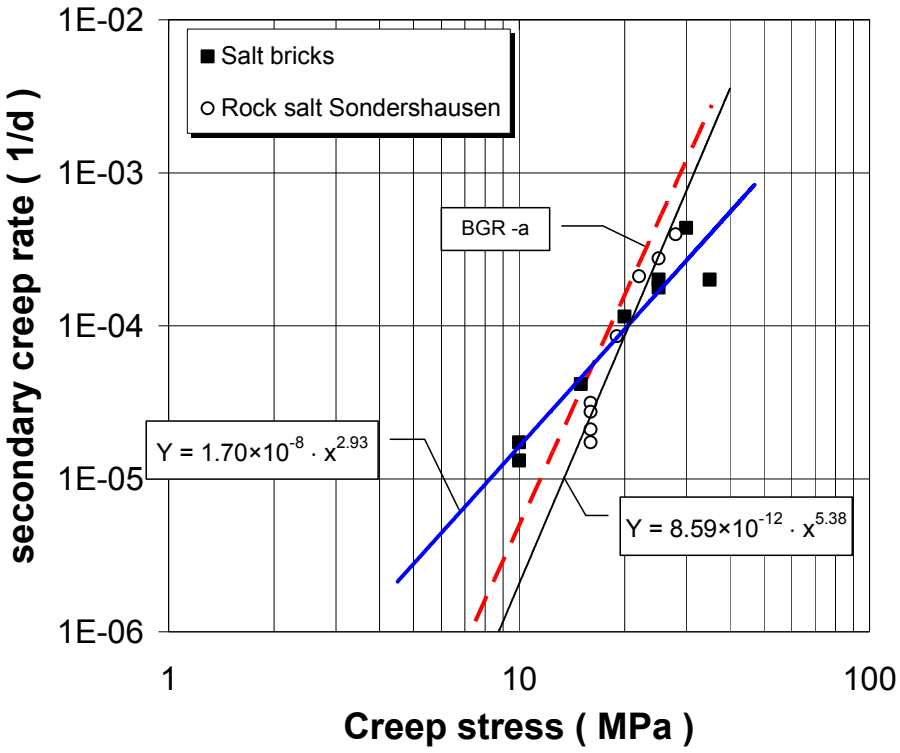

Figure 3-3. Measured steady-state creep rates in salt bricks compared to natural rock salt samples from the salt mine Sondershausen (Na2) and the BGRa-creep-law.

A comparison of the creep parameters of the investigated salt bricks with the creep law BGR-a and creep parameters of Staßfurt rock salt from Sondershausen (Anhydrite region) shows clearly the faster creep of crushed rock salt in the range of small σ_{diff} < 15 MPa than the reference curves (Figure 3-3).

For a better understanding of the humidity effects on the long-term properties hydrostatic compaction tests (three wet and two dry) with an overall duration of at least more than one year were performed in the creep rigs at σ_{hyd} = 3, 10 and 20 MPa respectively. In addition, in the dry experiments the temperature was varied to estimate the activation energy.

Because information on the volumetric strain is unreliable in granular salt precise shape measurements of the samples (once during and after the test) regarding sample length, diameter and volume were made which facilitate an estimate of the volumetric strain only based on the continuous measurement of ε_1. The sample parameters and experimental conditions are summarized in Table 3-1. The time dependent compaction behavior compared to the respective sample porosities is shown in Figure 3-4.

Table 3-1: Sample parameters of the long term compaction experiments.

No	σ_{hyd} [MPa]	ρ [g/cm^3]	w [wt.-%]	ε_1 [%]	ε_V [%]	$\varnothing_E$ [%]
208/36	3	1.992	0.42	3.10	6.32	2.18
208/38	10	1.975	0.65	3.44	6.77	2.08
208/39	20	1.973	0.46	3.33	7.91	1.12
208/40	10	1.974	0.07	0.43	0.98	8.25
208/37	20	1.975	0.06	1.26	3.09	6.24

Abbreviations: ρ = density; w = water content; $\varnothing_E$ = final porosity.

Comparing the various curves it can be clearly seen that besides the loading conditions the water content is obviously the key factor for the compaction behaviour. But the efficiency of the compaction process changes with progressive compaction.

Referring to the non-moisturized samples (i.e. “dry”), it is documented by the test results that they do not reach a significant compaction (e.g. in the order of several %) within the whole test period. An approximation of the time dependent compaction curves via a power function leads to an estimate of the necessary time for reaching significant compaction. In the non-moistened samples the necessary time for reaching a reference state of approx. 6 % porosity would be around 8 – 9 years (for 20 MPa) and around 180 years (for 10 MPa) respectively.

In contrast, the necessary time periods in moistened salt brick samples are only 9 days at σ_{hyd} = 20 MPa, 14 days at σ_{hyd} = 10 MPa, and around 90 days at σ_{hyd} = 3 MPa, respectively, indicating very rapid porosity reduction also at low stress conditions.

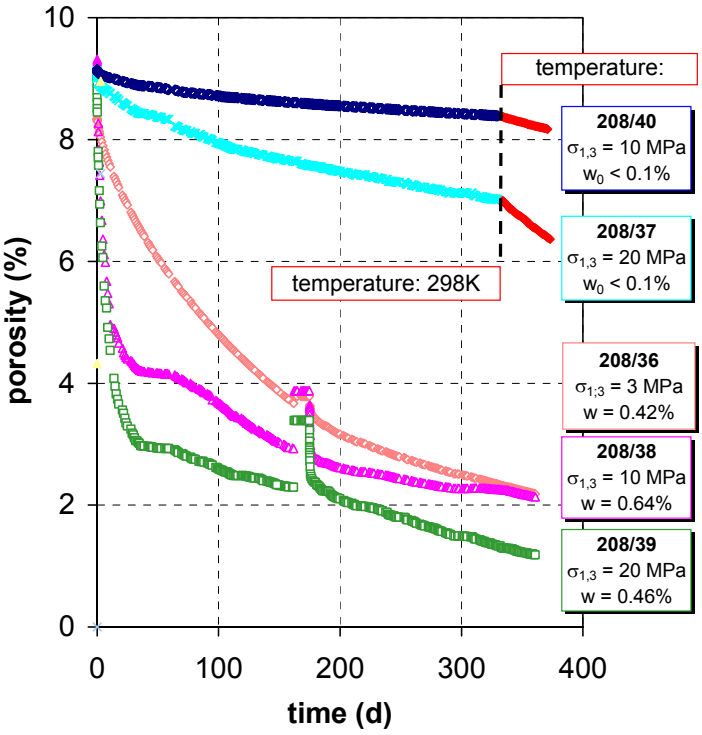

Figure 3-4. Results of hydrostatic compaction creep tests on cylindrical samples of pre-compacted salt brick material. Note effect of added water content (w). After 162 days the experiments were interrupted and the wet samples were built out to evaluate the shape parameters for the calibration of the volumetric strain approximation (as described before).

With progressive compaction, in both wet samples deformed at σ_{hyd} = 10 MPa resp. 20 MPa, the initial compaction proceeds very fast until after around 50 days a saturation state at a remaining porosity level of $\varnothing \leq 4\%$ is reached. Then the compaction is progressively impeded. In contrast, the time dependence of the sample 208/36 (σ_{hyd} = 3 MPa) is characterized by transient behaviour over about 200 days until the final phase of nearly stationary deformation is achieved corresponding to those at higher stresses.

Additionally in the dry experiments the temperature were varied (from 25°C to 55°C) which allows an estimate of the activation energy which was found to be in the order of Q = 39 kJ/mol (0.4 eV), such value is typical for material transport in rock salt by diffusion (e.g. Hunsche & Schulze 1994).

3.3 Permeability tests on dry samples

In addition to the overall compaction behaviour knowledge about changes of transport properties in highly compacted granular salt undergoing deformation is of utmost importance regarding their sealing efficiency. In supplement of the strength tests (see chapter 3.1) three triaxial deformation tests at 2, 5 and 10 MPa confining pressure with stepwise permeability measurements were performed. Specific sample parameters are summarized in Table 3-2.

The general deformation characteristics in these tests correspond to the behaviour observed in the standard tests. Whereas in the low confining pressure experiment (sample 26, σ_3 = 2 MPa) a minimum in the volumetric strain occurs (at ε_1 = 2.4% with ε_V = -0.6%, σ_{diff} = 34 MPa), followed by subsequent dilatancy, in both other samples deformed at σ_3 = 5 resp. 10 MPa the overall deformation is associated with compaction down to 1 - 2% remaining porosity. Remarkably, in the last step sample 28 was deformed during application of a gas pressure (p_1 = 7 MPa, σ_3 = 10 MPa). The pore pressure effect lowered the horizontal stress to $\sigma_{3;eff} \approx$ 3 MPa and resulted in a rapid change of deformation style from compaction to dilatancy associated with a volume increase of around 0.8% (Table 3-2). In addition, after the experiment the sample displays clear indication of the development of shear failure resulting in two distinct fracture sets, which emphasizes the importance of the effective stress concept in porous granular salt.

Table 3-2: Experimental conditions for strength tests with stepwise permeability measurements.

Specimen No.	σ_3 [MPa]	ε_{max} [%]	$\varepsilon_{Vol(end)}$ [%]
26	2	22.88	+1.67
25	5	29.98	-6.68
28	10	39.91	-8.37
28*)	3 (= $\sigma_{3\text{-eff}}$)	41.64	-7.60
27	0.33 · σ_1	4.00	-2.58

*) Deformation during continuous application of a gas pressure p_p = 7 MPa resulting in the onset of dilatancy

During the constant rate deformations test the experiments were interrupted (in steps of two to three percent axial deformation) and the stationary gas-permeability k was measured with N_2 at each deformation step (including the initial value ε_1 = 0%). In summary, nearly 40 mea-

surements were recorded. The respective porosity ∅ values were determined on the basis of the initial porosity, as estimated from the sample density and the volumetric strain. The results of the various tests are depicted in Figure 3-5 as a double logarithmic diagram of k vs. ∅.

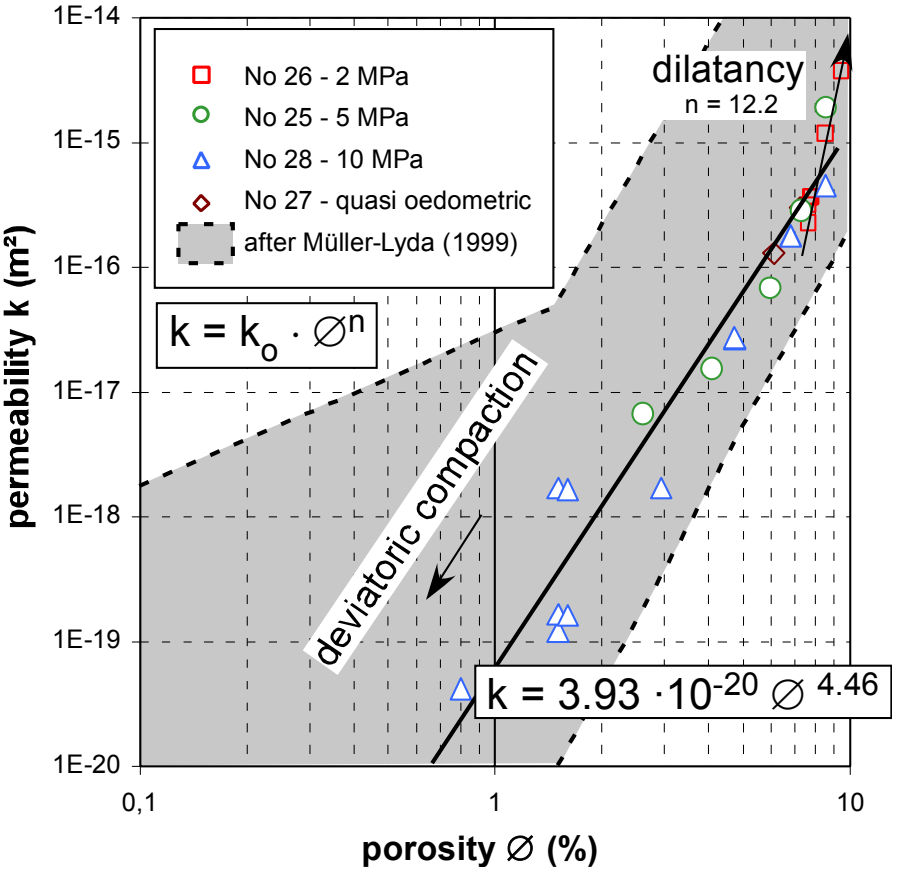

Figure 3-5. Porosity-permeability data for dry salt brick material deformed in compression under triaxial loading conditions at room temperature. In addition, the ranges of the datasets of Müller-Lyda (1999) are schematically indicated.

Although the data show some scattering, the general permeability-porosity dependency obtained during the deviatoric compaction corresponds to former results and falls into the variation field, reported by Müller-Lyda (1999). In detail, two opposite trends for the porosity/permeability relationship can be distinguished. Whereas in the low pressure range (σ_3 = 2 MPa) where dilatant deformation proceeds a steep increase of both, permeability and porosity occurs (n = 12.2), the opposite trend is observed at higher pressures ($\sigma_3 \geq 5$ MPa) but with smaller slope. Using a simple power-law ($k = k_0 \cdot \varnothing^n$) relation the compaction behaviour can be expressed with:

$$k = 5.7 \cdot 10^{-20} \cdot \varnothing^{4.31} \quad (3\text{-}2)$$

The observed exponent n for compaction agrees very well with the mean value of 4.5 obtained by Müller-Lyda (1999). However, the last author mentioned that in wet granular salt n is significantly higher (up to 5.5) but that generally at porosities lower than ~0.5% and in a permeability range of around 10^{-20} m^2 n becomes significantly smaller than 4.

3.4 Capillary threshold effects in a wet sample

If water is present at the grain boundaries and gas will penetrate into the rock matrix of the salt bricks two-phase flow will occur which is associated with capillary effects. Fluid transport is then controlled by the interfacial tension of the fluids involved, the wettability of the solid surface (wetting angle) with respect to the fluids, and the structure of the pore system.

According to the Washburn equation (Washburn 1921) intrusion of a non-wetting fluid into a cylindrical capillary of radius r only occurs if the capillary pressure p_c (i.e. the pressure difference between the two immiscible fluids with p_1 and p_2) within a pore is exceeded:

$$p_c = p_2 - p_1 = -\frac{2 \cdot \gamma \cdot \cos\theta}{r} \quad (3\text{-}3)$$

Here γ is the interfacial tension (N/m), and θ the wetting angle (degrees) and r is the radius (m) of the ideal cylindrical pores.

As schematically depicted in Figure 3-6 the capillary sealing efficiency of a porous medium with a heterogeneous pore system (i.e. a given pore-size distribution) is characterised by the "break through" or "threshold pressure" (p_T). This term refers to the excess pressure in the non-wetting phase at which the wetting phase is displaced to an extent that the percolation threshold is exceeded and continuous flowpaths of non-wetting phase develop across the pore system. These flow-paths will comprise the largest interconnected pores, which offer the least resistance to capillary displacement. At this stage the flow of the non-wetting phase will be focused and restricted to a small portion of the interconnected pore system. If the excess pressure increases further, additional fluid flow pathways will develop across the porous medium, thus increasing the effective permeability to the non-wetting phase and the non-wetting phase saturation.

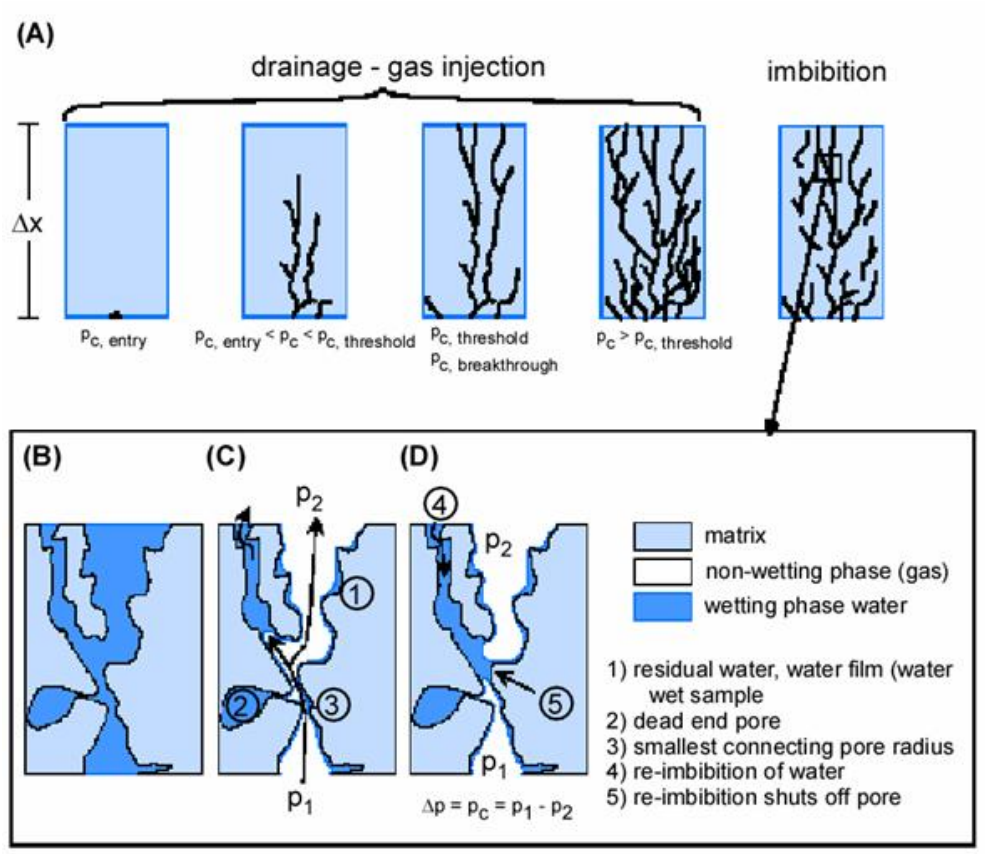

Figure 3-6. Two phase flow in porous media. (a) Stages of capillary gas breakthrough (drainage) and re-imbibition process in fine-grained rocks (schematic); (b) initially water-saturated sample; (c) gas breakthrough, (d) re-imbibition (modified after Hildenbrand 2003).

The coupled transport and mechanical properties of highly compacted and moistened granular salt were investigated in a multi-stage deformation experiment, similar to those described before, but using a wet salt brick sample (no. 208/41). Its internal humidity content was estimated to be in the order of 1.3 wt.-% corresponding to the other data, resulting in a partially or, referring to the accessible pore space, nearly saturated pore space.

The gas-injection experiment consists of several stages of hydrostatic compaction and controlled axial deformation, respectively, which here can not described in detail. Threshold pressure was determined in relaxation phases (ε_1 = const.) directly by incrementally increasing the pressure of gas in contact with the end of a fully saturated core sample and observing the pressure at which gas first penetrates through the core (the minimum resolution of the used flow meter is 0.2 ml/min) (Figure 3-7). This approach gives the pressure required for the

incipient development of interconnected gas flow paths through the pore network. After reaching a stable gas flow through the sample the gas permeability is measured as reference for the later comparisons (here described as intrinsic permeability). Because after this step the sample is further compacted resulting in a porosity decrease the effects of partial water loss during the gas injection test can be neglected.

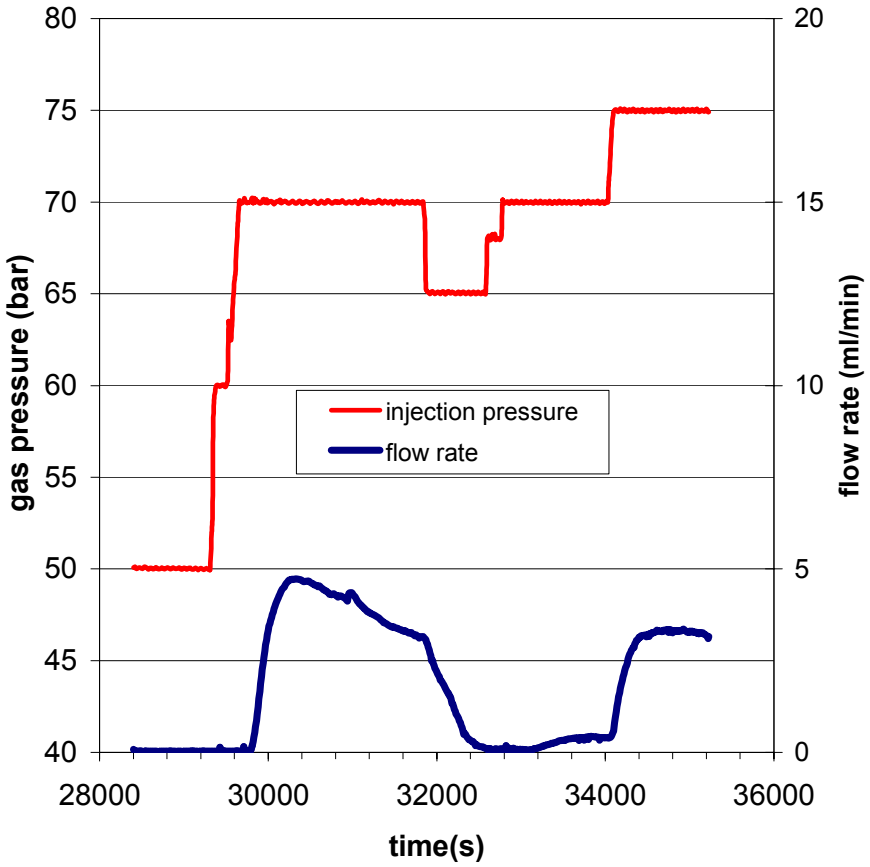

Figure 3-7. Example for the determination of the capillary gas threshold pressure. Stepwise increase of the injection pressure with concomitant gas flow measurements (ε_1 = 11.3%, ε_{vol} = 5.5%). Note, that the steep increase of gas flow occurs in the gas injection pressure step to 70 bar (1. cycle) resp. shifted to 75 bar in the 2. cycle indicating time-dependent compaction.

The results from at least 9 gas injection tests on the salt brick sample 208/41 undergoing deformation are shown in Figure 3-8 in relation to literature results from different lithologies, i.e. sedimentary rocks.

As concluded by various authors (e.g. Marshal et al. 2005) a clear trend between threshold pressure and so-called intrinsic permeability is seen for the different lithologies, but the spread of the data is enormous. For comparison, we indicated the ranges of threshold pressure correlated with permeability for various lithological salt portions as estimated by Davies

(1991). It has to be mentioned that these estimates are only based on the overall relationship for sedimentary rocks and the known permeability ranges of various salt types resp. salt with different disturbance state.

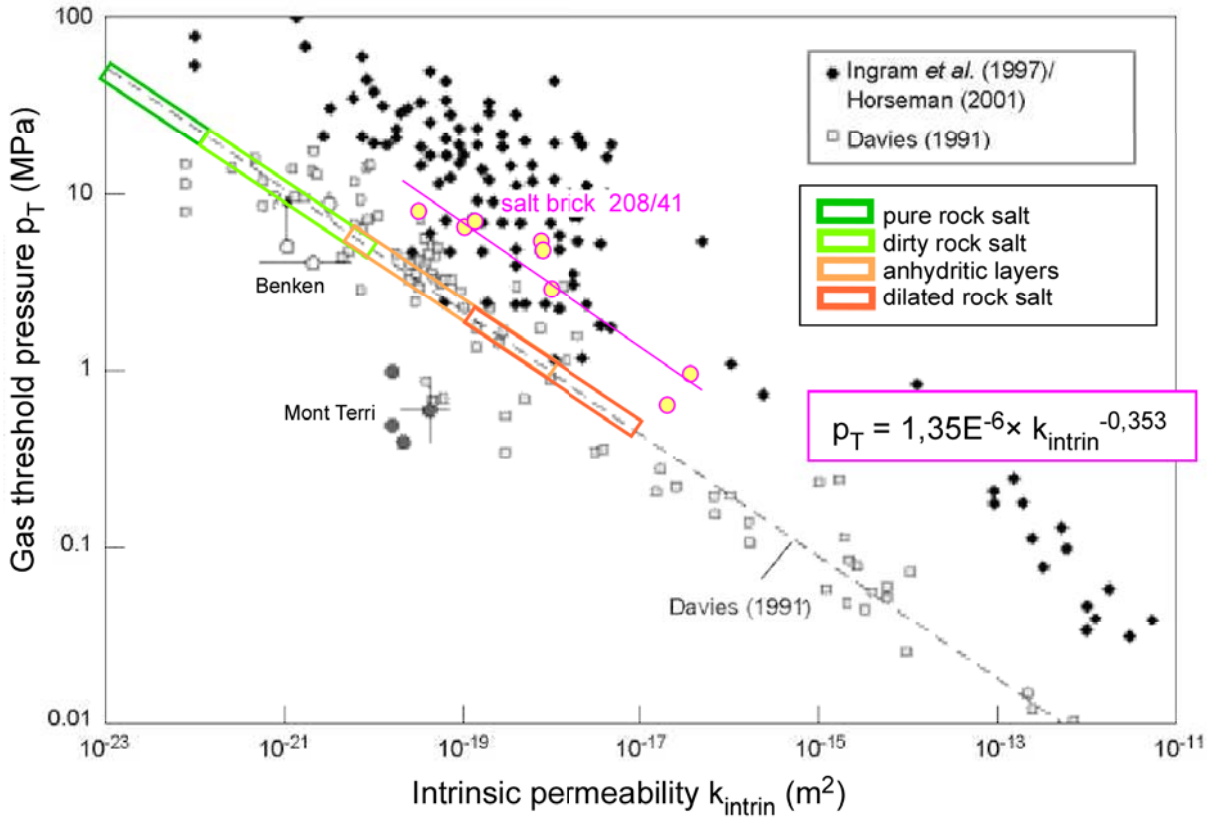

Figure 3-8. Relationship between gas threshold pressure and intrinsic permeability for various low permeability rock formations (claystones, shales, sandstone) (modified after Marshal et al., 2005 – for the various references see the later authors). In addition, the ranges of threshold pressure correlated with permeability for various lithological salt portions are indicated (as estimated by Davies 1991). The results obtained here are shown by big magenta-rendered yellow circles.

In a first approximation, the relationship between permeability (k_{intrin}) and gas threshold pressure (p_T) for the moistened salt brick corresponds in a double-logarithmic diagram to a linear trend which is slightly higher than the prognosis postulated by Davies (1991) as presented in Figure 3-8:

$$p_T = 1.35 \cdot 10^{-6} \cdot k_{intrin}^{-0.35} \qquad (3\text{-}4)$$

Because our experiments are short term tests, the test duration during the various injection tests may not be sufficient to detect the gas-breakthrough already in the investigated time interval which would result in an overestimation. However, taking this in mind our results representing synthetic and highly compacted granular salt correspond reasonably well to the published data.

3.5 Shear-tests between dry or wet salt-brick surfaces

For a performance assessment of the long-term sealing or buffer system build up by salt bricks under investigation it is also necessary to determine the contact properties between these bricks and between the bricks and host rock, i.e. rock salt. Such discontinuities can act as mechanical weakness zone or preferred pathways. For the mechanical behaviour of interfaces the relevant variables are stress traction vector with one normal component (σ_n) and one tangential in a simple 2-dimensional stress field, i.e. τ (or two tangential in 3D), and the conjugate "strain" variables are the corresponding relative displacements, as shown schematically in Figure 3-9.

However, such stress conditions can be only realized in direct shear tests, which are therefore of urgent need to reproduce slip between various materials. For realization of required shear tests a modern MTS-shear test system is available at the IfG (Figure 2-1). It is a high-response servo-hydraulic system with digital control technology, strain measurement equipment mounted onto the specimen and programmable control modes, enabling new types of test procedures to be performed.

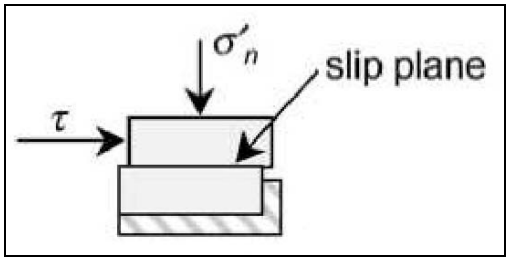

Figure. 3-9. Loading geometry in direct shear test

To investigate the shear strength between the various contacts, halved salt bricks were stacked one on the top of the other and covered with a plastic foil to protect them against dissolution by the wet concrete that fixes the samples in the shear boxes. So, the contact planes between the two bricks are exactly perpendicular to the shear direction in the centre of the shear box. Samples for the second test row were similarly prepared. Instead of two salt bricks (or salt brick halves) a salt brick was arranged on a rough contact plane of a host rock block (i.e. medium-grained rock salt).

On both contact types two series of multiple-step shear tests were performed aiming on the properties of the dry and wet interfaces:

(1) Properties of dry interfaces: Determination of shear strength with a multiple-step shear test by cyclical shearing of one sample half (forward/backward) with several normal stresses (σ_n = 0.5, 1, 2, 4, and 6 MPa).

(2) Effect of wetting: Realization of shear tests between samples with moistened surfaces at various loading times and normal stresses. - Investigation of efficiency of healing processes.

Table 3-3: Overview about results of shear tests between salt bricks under dry conditions.

healing period [hours] with σ_N = 10 MPa	normal load σ_N while shearing [MPa]	maximum shear stress τ_{MAX} [MPa]	residual strength [MPa]
16	1.0	0.58	0.30
16	1.0	1.26	0.36
16	4.0	3.18	0.78
70	4.0	1.90	0.94
94	1.0	1.66	0.43
94	4.0	3.68	0.59

Table 3-4: Overview about shear test between salt bricks under wet conditions.

healing period [hours] with σ_N = 10 MPa	normal load σ_N while shearing [MPa]	maximum shear stress τ_{MAX} [MPa]	residual strength [MPa]
16	1.0	1.28	0.39
16	2.5	2.60	0.40
16	4.0	3.25	1.00
70	1.0	1.16	0.33
70	2.5	3.40	0.49
70	4.0	6.15	3.46
94	2.5	4.40	0.53
94	4.0	6.19	ca. 4.0

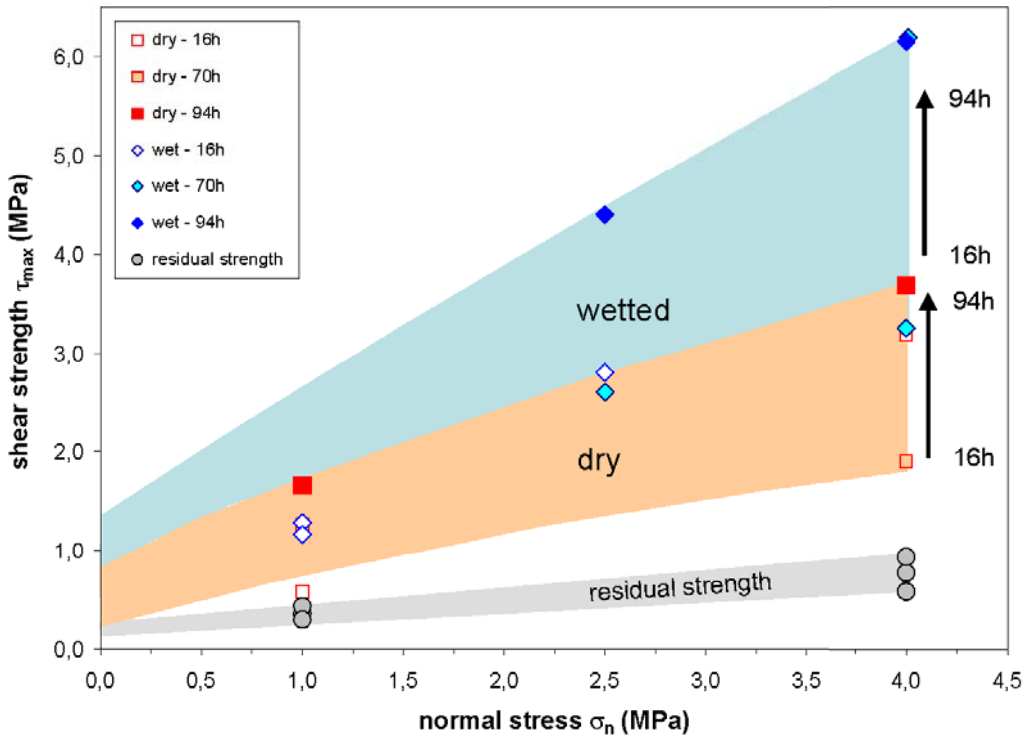

Figure 3-10. Shear strength characteristics of lab-dry and moistened brick-brick and brick-rock salt contacts. Healing effects are promoted by the presence of moisture and increase systematically with stationary ageing over 16, 70 and 94 hours at fixed normal stress (multiple step tests at constant normal stress).

In appraisement of the various results presented in Figure 3-10 it is obvious that in each experiment the stress-depended strength of discontinuity plane can be described by the MOHR-COLOUMB criterion. As result the shear resistance at critical stress conditions (shear failure) is expressed by a linear dependency of cohesion (c) and angle of friction (φ):

$$\tau_f = c + \sigma_f \cdot \tan \varphi \qquad (3\text{-}5)$$

The respective results are given in Table 3-5.

Table 3-5: MOHR-COULOMB-parameters from shear tests for various interfaces.

Interface	Humidity state	c [MPa]	φ [°]
Saltbrick/saltbrick*)	dry	0.08 ±0.04	11 ±4
Saltbrick/saltbrick**)	wet - 16h	0.63	33
Saltbrick/saltbrick**)	wet - 94 h	1.00	34
Saltbrick/rocksalt**)	dry	0.00	~10
Saltbrick/rocksalt**)	wet – 16h	0.54	47

*) Tested in multi-stage shear tests with cyclical shearing (mean value of 6 exp.);**) Single shear experiment at each σ_n-stage.

Most important, under the influence of normal stresses, but only in wet samples interfacial cohesion forces (in the order of 0.5 – 1.0 MPa) and/or other strengthening effects are activated depending on the loading time and the moisture content of the contact. In contrast, on dry surfaces only a small healing or strengthening effect is recognizable, whereby the magnitude depends on loading time.

4 Crushed salt constitutive models

4.1 Material law selection

Referring to the use of crushed salt as the preferred backfill material in the salt concept numerous constitutive material laws describing crushed-salt deformation have been developed in the past. A comprehensive review concerning appropriate models for description of conditions relevant for the WIPP-site is given by Callahan et al. (1995). The authors identified at least 10 crushed-salt constitutive models from the literature search, which were separated into:

(1) empirical formulations, e.g. the Zeuch & Holcomb (Holcomb & Zeuch, 1988); Sjaardema –Krieg-Model (Sjaardema & Krieg, 1987)
(2) micromechanism-based, e.g. Spiers et al., 1989
(3) a visco-plastic approach, e.g. Liedke et al. (1986).

In general, all models are generalized to three-dimensional states of stress to include the effects of mean and deviatoric stress and modified to include effects of temperature, grain size, and moisture content. Among the various models, three were tentatively selected by Callahan et al (1995) for further examination, i.e. the models mentioned in the sections (1) and (2).

In an update report, Callahan et al. (1998) presented modifications to the WIPP specific constitutive model for describing the consolidation of crushed salt with time. Two mechanisms -- dislocation creep and grain boundary diffusional pressure solution -- defined previously but used separately are combined to form the basis for the constitutive model governing the deformation of crushed salt.

In addition, an extended database consisting of creep consolidation tests, hydrostatic consolidation and shear consolidation tests conducted on Waste Isolation Pilot Plant and southeastern New Mexico salt was used to determine material parameters for the new constitutive model. Nonlinear least-squares model fitting to data from the shear consolidation tests and a

combination of the shear and hydrostatic consolidation tests produced two sets of material parameter values for the model. The change in material parameter values from test group to test group indicates the empirical nature of the model but demonstrates improvement over earlier work with the previous models. Key improvements were the ability to capture lateral strain reversal and better resolve parameter values.

Recently within the framework of the BAMBUS[1] I (Bechthold et al, 1999) and BAMBUS II (Bechthold et al., 2004) projects, comprehensive investigations and modelling were performed to confirm and improve existing constitutive models used to predict the long-term evolution of backfill porosity and excavation disturbed zone (EDZ) in and around disposal drifts in a HLW repository in geological salt formations.

A variety of Finite Difference and Finite element codes have been used by the different research teams working in the BAMBUS projects to numerically model the thermomechanical behaviour of crushed salt and salt rock in repository relevant conditions, e.g. ANSALT, ANTEMP, FLAC, ADINA, ANTIC, GEOMEC, MARC and CODE_BRIGHT (Bechthold, et al. 2004). These are often public or commercial codes that allow implementation of constitutive laws for rocksalt and crushed salt.

In the BAMBUS II calculations the porosity of the backfill under consideration ranged from 35% to 20%, whereby temperatures are very well calculated, but predicted drift-closure has larger errors ranging from 10% to 90%, and the predicted stresses in the backfill exhibit by far the largest errors.

In conclusion, various numerical tools are available and numerical efforts devoted to modelling several laboratory and in situ tests were significant but the constitutive models have not been tested in the porosity range between 10% and 1%. However, following the experiences made in the BAMBUS-projects we selected the following constitutive modells:

- The Itasca crushed-salt constitutive model, i.e. the modified WIPP-reference creep law
- The Hein-Model
- The Zhang-Model
- The Spiers-Model

Unfortunately, only the ITASCA crushed-salt constitutive model and the Hein-model are implemented in *FLAC*^{3D}, which was originally foreseen as the tool to perform model calculations. *FLAC* software has been used for numerical modeling of the underground excavations

[1] **B**ackfill **a**nd **M**aterial **B**ehaviour in **U**nderground **S**alt Repositories

at the WIPP since 1991. *FLAC* is a two- respectively *FLAC*^{3D} is a three-dimensional explicit finite difference code that simulates the behaviour of rock and soil-lie structures. For example the WIPP Reference Creep Law is built into *FLAC* and has been verified to Nuclear Regulatory Commission standards (Itasca, 1995).

Therefore, to extent the frame of investigations the respective constitutive equations of the four investigated models were implemented in *Mathcad* 8.0 for doing numerical calculation on the base of existing parameter sets. In a second step new parameter sets were fitted to the existing data base. *Mathcad* (originally written *MathCAD*) is desktop software for performing and documenting engineering and scientific calculations which is now distributed by Parametric Technology Corporation (http://www.ptc.com/). All necessary functions and operators are built-in in *Mathcad*. In additions, as a special advantage *Mathcad* allows a simple solving of differential equations, which facilitates calculation of the volumetric strain resp. porosity evolution in the long term creep tests.

In the following, in the respective chapters a short description of each constitutive model and of adaptation results are given. A comprehensive documentation of the constitutive equations and the realized adaptation studies are reported in the deliverable 3.5.6 (IFG, 2007).

4.2 ITASCA crushed-salt constitutive law (CS-ITASCA-model)

A crushed-salt constitutive model is implemented in the ITASCA-program family (*FLAC FLAC*^{3D}*, UDEC and 3DEC*) to simulate volumetric and deviatoric creep compaction behaviour. The model is a variation of the WIPP-reference creep law and is based on the model described by Sjaardema and Krieg (1987), with an added deviatoric component as proposed by Callahan and DeVries (1991).

Our long term hydrostatic compaction creep tests show a strong temperature dependency of the porosity rate respectively the compaction strain rate. In contrast to this observation the ITASCA crushed-salt constitutive equation for the compaction strain-rate is not able to consider temperature dependency.

The advantage of the ITASCA crushed-salt constitutive law compared to the other examined laws, except for SPIERS model, consists in the independence of the material parameter values from the initial porosity ρ_0 of the pre-compacted crushed salt material.

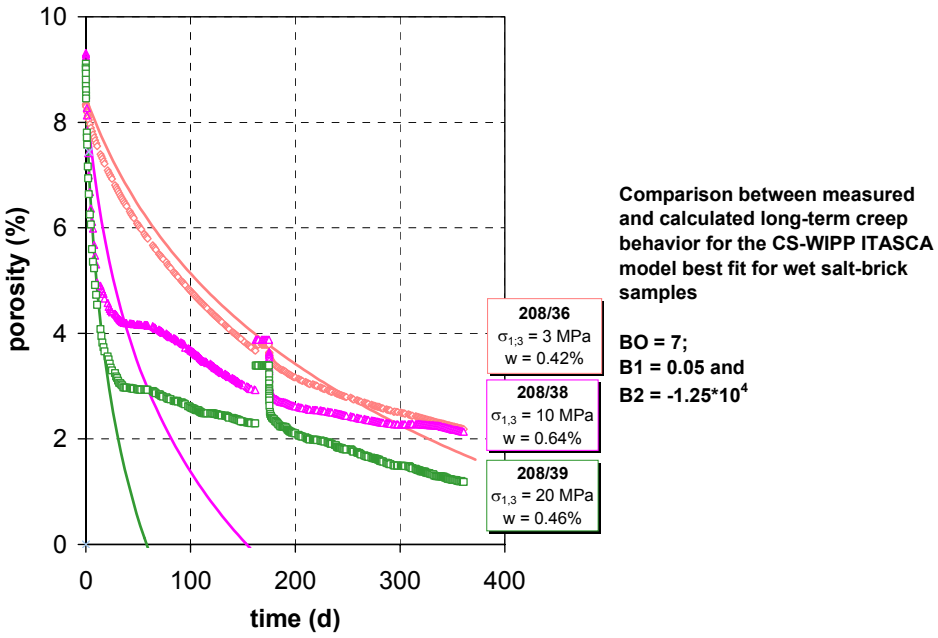

Figure 4-1. Comparison between measured and calculated long-term creep behaviour for the CS-WIPP ITASCA model, calculations performed with best fit for wetted salt brick samples. Porosity vs. time (symbols indicate the measured behaviour, continuous lines the calculated one, colours mark the stress conditions for the creep-test)

The porosity-time behaviour for isotropic long term creep tests show for the ITASCA constitutive equation that the final density of undisturbed salt can be reached in a comparatively short time and finite mean stress (Figure 4-1), whereas the laboratory investigation show an asymptotical approach to this state also for long time and high mean stresses. This is a principal deficiency of the model which prevents to reflect the observed stress dependency of the hydrostatic creep behaviour in the low porosity region.

In summary we can conclude that the ITASCA crushed-salt constitutive law is not suitable to describe the compaction behaviour of the pre-compacted crushed-salt bricks in the low porosity region.

4.3 HEIN constitutive law

The constitutive relation of crushed salt proposed by Hein (1991) was adopted, because three participants of the BAMBUS II – project (Bechthold et al., 2004) also used this model (DBE, FZK and NRG). Fortunatly this constitutive model for the crushed salt behaviour is implemented in the ITASCA *FLAC*^{3D}-program code so it could easily examined.

It is based on a viscoplastic formulation and considers both volumetric and deviatoric strain rates under hydrostatic and deviatoric stress conditions. The elastic behaviour is determined by porosity depending elastic properties, with low bulk and shear modulus at the beginning of the compaction, reaching the values of compacted material at total compaction. The viscoplastic part is a combined hydrostatic-deviatoric law. The material parameter values are derived from extensive triaxial tests (e.g. Korthaus, 1996). A more detailed description of the HEIN model can be found in Hein (1991) and Lerch (1999).

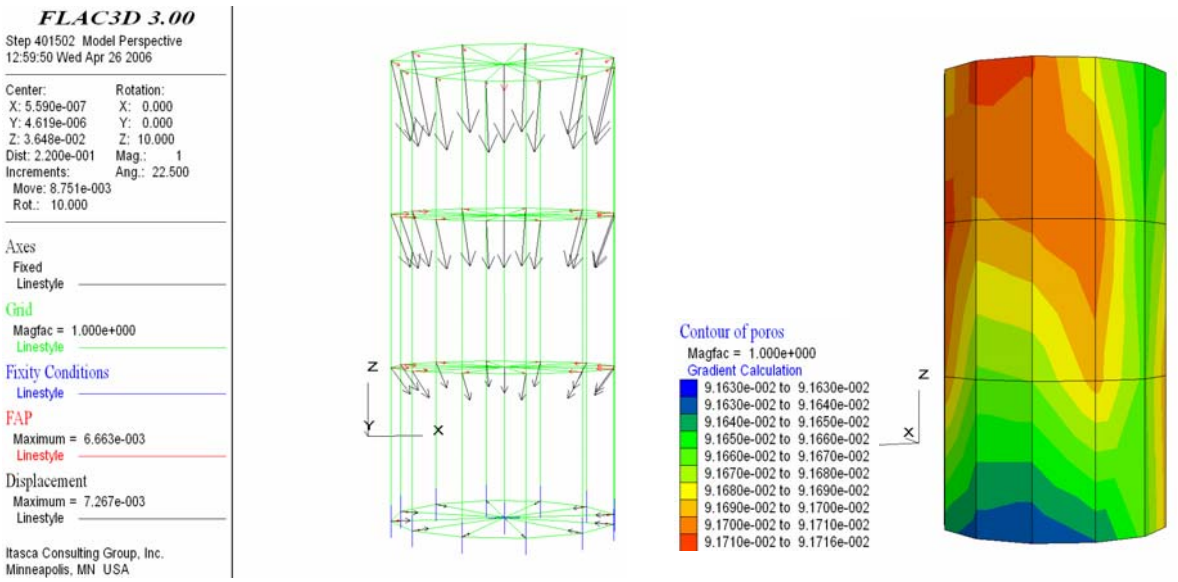

Fig. 4-2. *FLAC3D*-sample model to perform recalculation of creep tests with the HEIN constitutive model. (green lines indicate the chosen grid, red arrows the acting forces, the blue lines the fixity conditions and the black arrows the displacements to reach the initial porosity of the salt bricks).

In addition to the above described semi-analytical investigations with *Mathcad* 3D-numerical calculations were performed with the same parameter set. For these calculations an ITASCA *FLAC*^{3D}-model with the real cylindrical sample geometry (diameter 4 cm height 8 cm) was developed. The hydrostatic pressure acts on the entire sample surface excepting the upper end face where vertical displacements are restricted, see Figure 4-2.

The HEIN-model allows recalculating the observed temperature dependency of the porosity rate respectively the compaction strain rate.

Similar to CS-WIPP-ITASCA-model the performed comparisons show for the HEIN-model that the stress-dependency, n, is too strong. Furthermore the calculated porosity-time curves show for the adapted parameter values that the final density of undisturbed salt can be

reached in a comparatively short time and at real hydrostatic stresses (Figure 4-3), whereas the laboratory investigations show an asymptotical approach to this state also for long times and high mean stresses. This is as well to the ITASCA-model a principal deficiency of the HEIN-model which prevents to reflect the observed stress dependency of the hydrostatic creep behaviour in the low porosity region.

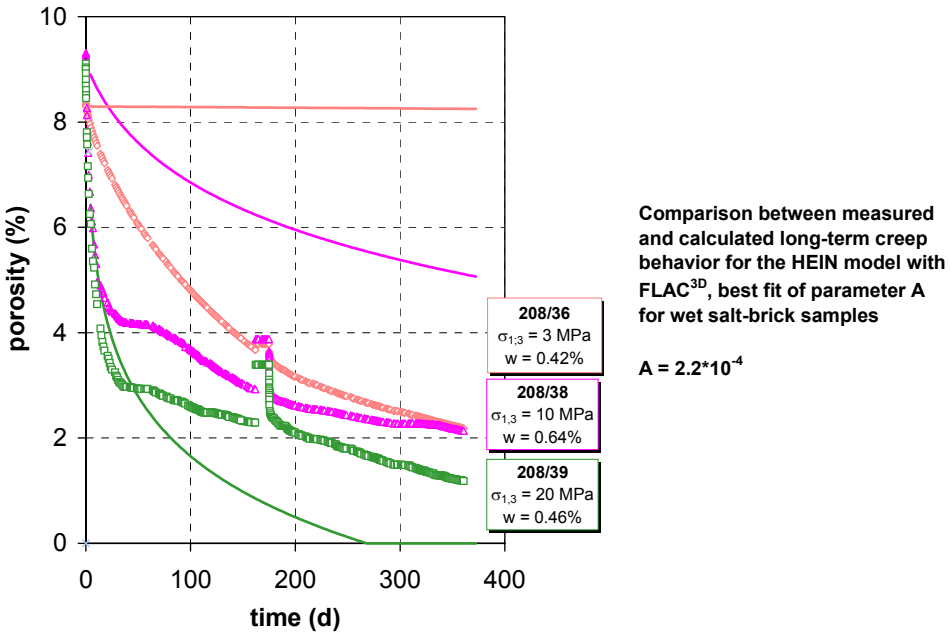

Figure 4-3. Comparison between measured and calculated long-term creep behaviour for the HEIN model, calculations performed with FLAC^{3D} best fit for parameter A and wet salt brick samples. Porosity vs. time (symbols indicate the measured behaviour, continuous lines the calculated one, colours mark the stress conditions for the creep-test)

A further disadvantage of the HEIM-model compared to the ITASCA crushed-salt constitutive model consists in the necessity to include in the calculation procedure the pre-compaction process of the salt bricks to the initial porosity, ϕ_0, of the crushed salt material, whereas the parameter set for the constitutive law must be deduced from the initial un-compacted crushed salt material with a comparatively high porosity. Due to this reason we can conclude that also the HEIN crushed-salt constitutive law is not suitable to describe the compaction behaviour of the pre-compacted crushed-salt bricks.

4.4 ZHANG constitutive law

In the BAMBUS I – project ZHANG's (Zhang et al., 1993) model was used by BGR as an enhanced version based on phenomenological and physical assumptions (Bechthold et al., 1999). Furthermore this constitutive law for the crushed salt behaviour was utilized by the IfG to describe several crushed salt backfill materials.

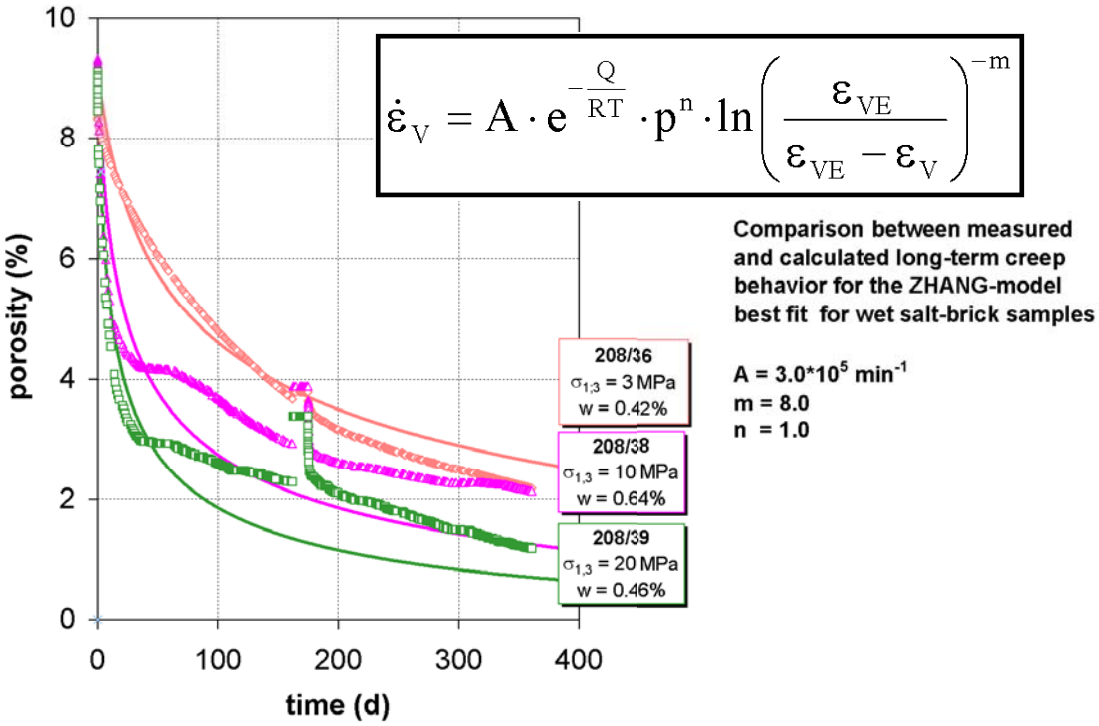

Figure 4-4. Comparison between measured and calculated long-term creep behaviour for the ZHANG model, calculations performed with best fit for wetted salt brick samples. Porosity vs. time (symbols indicate the measured behaviour, continuous lines the calculated one, colours mark the stress conditions for the creep-test)

The formulation of ZHANG-model includes the observed temperature dependency of the porosity rate respectively the compaction strain rate in form of the physical founded Arrhenius approach. The dependency of compaction is a phenomenological founded approach.

As a first statement it has to be mentioned, that similar to the CS-ITASCA-model and the HEIN-model our results demonstrate that the original stress-dependency (n = 5 - 7) which was determined for material with a comparatively large porosity is too strong. However, unlike to the CS-WIPP-ITASCA-model and the HEIN-model the calculated porosity-time

curves show for the adapted parameter values a transitional behaviour from a steep decrease to a progressively lower change, i.e. in accordance of the model-calculations of the ZHANG-model and the laboratory results the low-porosity behaviour of the salt bricks is characterised by an asymptotical shape slowly approaching a final state of compaction after sufficient long times and high mean stresses (Figure 4-4). This means that at real hydrostatic stress conditions the final density of undisturbed salt cannot be reached in limited time, as may be inferred from the two other models. This is in principal the most important advantage of the ZHANG-model which allows reflecting the observed stress dependency of the hydrostatic creep behaviour in a good manner.

However, in difference to the ITASCA crushed-salt constitutive law also the ZHANG-model requires as a disadvantage, similar to the HEIM-model, the necessity to include in the calculation procedure the pre-compaction process of the salt bricks to the porosity ρ_0 of the salt brick material, whereas the parameter set for the constitutive law must be deduced from the initial un-compacted crushed salt material with a comparatively high porosity.

In summary we can conclude that the phenomenological founded ZHANG crushed-salt constitutive law is suitable to describe the compaction behaviour of the pre-compacted crushed-salt bricks in a first approximation but the necessity to include the pre-compaction history is a disadvantage.

4.5 SPIERS constitutive law

In the NFPRO – project Spiers (e.g. Spiers et al. 2005) proposed a mechanism-based microphysical constitutive model for the crushed salt behaviour in the low porosity region (10 - 1%) which has been developed over the experiences gained in the last two decades. Nevertheless, the actual microphysical model, as presented in detail by Zhang & Grupa (2006) is preliminary, as mentioned by the authors, and needs, therefore, further improvement by means of comparison with the data from future experiments. However, from our feeling it's also in its present an important step for understanding the granular salt behaviour in the low-porosity range.

The formulation of SPIERS mechanism-based constitutive model for pressure solution creep includes the observed temperature dependency of the porosity rate respectively the compaction strain rate in form of the physical founded approach for pressure solution. The dependency of compaction is a geometrically founded approach.

Similar to the other analyzed models recalculations with the dislocation creep models it has been confirmed that a stress-dependency with n = 5 is too strong. In accordance to the CS-ITASCA-model and the HEIN-model the calculated porosity-time curves are not compatible with the observed asymptotical behaviour when a remaining porosity in the order of some few percent is reached. The model result of a steep porosity decrease only pretends an effective compaction behaviour to an infinitesimal low porosity, which not supported by the experimental results (Figure 4-5). Therefore, this is a deficiency of the SPIERS pressure solution-model which do not allow to simulate the observed stress dependency of the hydrostatic creep behaviour in the low porosity region (ϕ < 3%). Obviously in this region a so fare unknown mechanism hinders the further compaction.

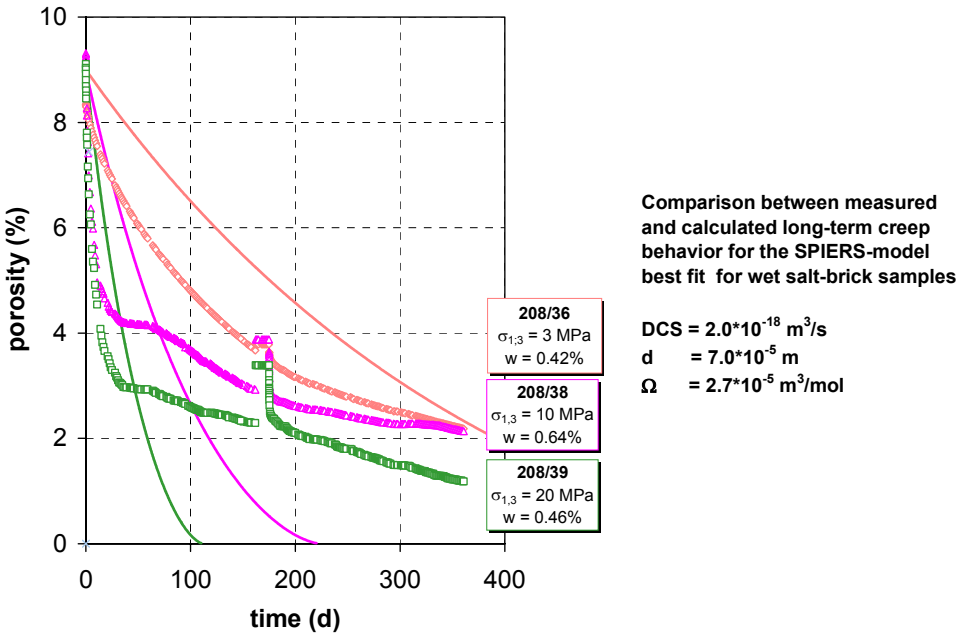

Figure 4-5. Comparison between measured and calculated long-term creep behaviour for pressure solution creep SPIERS mode, calculations performed with best fit for wetted salt brick samples. Porosity vs. time (symbols indicate the measured behaviour, continuous lines the calculated one, colours mark the stress conditions for the creep-test).

However, a fundamental advantage of the SPIERS pressure solution-model, like the ITASCA crushed-salt constitutive law is, that no pre-compaction process of the salt bricks to the porosity ρ_0 of the crushed salt material must be included in the recalculation algorithm.

In addition, the most important advantage of the SPIERS mechanism based pressure solution-model is the clear physical understanding of the dominating processes in the low porosity region of the compaction of highly pre-compacted salt bricks. But future effort is necessary

to enhance the mechanism-based pressure-solution model. Obviously for a wide grain size distribution a modification of the constitutive model is needed.

5 Mechanical contact plane properties between salt-bricks

5.1 Introduction

Focusing on the mechanical contact plane properties between salt brick itself respectively to the host rock contour, the classical description of the behaviour of such mechanical weakness planes is analogue to the strength properties of an intact rock the MOHR-COULOMB criterion were used to describe the discontinuity plane characteristics of a jointed rock, see chapter 3.5.

However, this concept described not the post-failure behaviour and may, therefore, not allow a sufficient representative description especially for dynamic conditions. Recently, MINKLEY (IfG, 2005a) developed a new shear model for bedding planes or contact interfaces, which implies the displacement-dependent and the velocity-dependent strength softening. It bases on the concept of CUNDALL & LEMOS (1990). The essential features of the shear model are:

- Dependence of the adhesive friction coefficient on the displacement rate of the shear process;
- The shear stress versus shear displacement curve approaches a “target” shear strength of the bedding or contact plane;
- The “target” shear strength remains constant until the softening region is reached, then it decreases with the progressing shear displacement.

Because this approach is assumed to provide a better understanding and contribution to a wider spectrum of the loading conditions the necessary parameters were derived on the existing database.

5.2 The Minkley-shear model

In the incremental formulation, the shear model can be described as follows. For the relationship between normal loading and normal displacement we use:

$$\Delta\sigma_N = k_N \cdot \Delta u_n \qquad (5\text{-}1)$$

where k_N is the normal stiffness and Δu_n is the normal displacement between the joint surfaces.

The model responds to the shear loading with an irreversible non-linear behaviour. The shear stress increment is calculated as follows:

$$\Delta\tau = F \cdot k_S \cdot \Delta u_s \qquad (5\text{-}2)$$

Here, k_S is the shear stiffness and Δu_s is the shear displacement parallel to the shear plane.

The factor F which reduces the slope is a function of the distance between the current shear stress τ and the peak shear strength τ_{MAX}:

$$F = 1 - \frac{\tau}{\tau_{MAX}} \qquad (5\text{-}3)$$

When taking into account the adhesive friction which is of essential importance for the bedding planes or contacts, the shear strength is found to be:

$$\tau_{MAX} = \mu \cdot \sigma_N + c \qquad (5\text{-}4)$$

with the friction coefficient:

$$\mu = \mu_K (1 + \Delta\mu) \qquad (5\text{-}5)$$

which consists of the coefficient of the kinetic friction:

$$\mu_K = \tan\left(\phi_R + i_0 \cdot e^{-K2\frac{\sigma_N}{\sigma_K}}\right) \qquad (5\text{-}6)$$

and the coefficient of the adhesive friction:

$$\Delta\mu = \Delta\mu_{vel} \cdot e^{-K1\frac{\sigma_N}{\sigma_K}} \qquad (5\text{-}7)$$

Here are: c = cohesion; ϕ_R = angle of residual friction; i_0 = upslide angle; σ_K = compressive strength in the contact area; and K1, K2 = curvature parameters. There effects on the kinetic and the adhesive friction components are proportional to the normal loading σ_N on the bedding plane. The cohesion diminishes only during very quick slide processes, whereas during a quite slow shear process the cohesive forces are maintained due to the specific characteristics of the salt which are covered by the rules of the physics of interfaces.

The dependence of the friction on the velocity v of the active shear process is represented by the following function:

$$f_{vel}(v) = \frac{1}{2}\left(1 + \tanh\left(b_S \cdot \log\frac{v}{v_K}\right)\right) \qquad (5\text{-}8)$$

Accordingly, the velocity-dependent extent inside the adhesive friction coefficient can be expressed by:

$$\Delta\mu_{vel} = \frac{\mu - \mu_K}{\mu_K} = \Delta\mu_{MAX} \cdot f_{vel} \qquad (5\text{-}9)$$

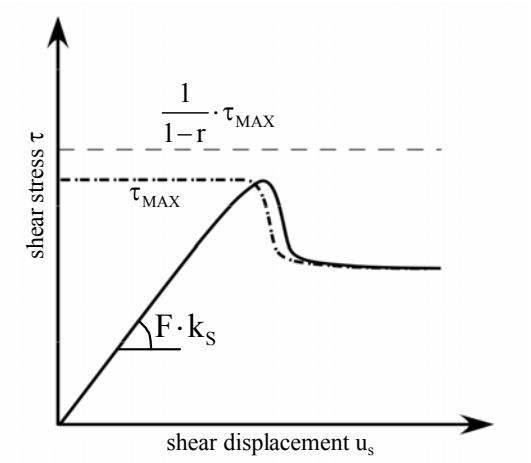

Figure 5-1: Shear model with strength softening.

Besides the velocity-dependent shear behaviour also a strength softening that depends on the passed shear displacement has been taken into consideration, in the developed shear model. As soon as the peak shear strength is approached, a reduction of the adhesive friction component occurs which depends on the plastic shear displacement. When the maximum shear strength τ_{MAX} has been approached up to a certain level r which must be preset, shear softening occurs if the following relationship is valid:

$$\tau \geq (1 - r) \cdot \tau_{MAX} \qquad \text{or} \quad F \leq r \qquad (5\text{-}10)$$

The reduction of the adhesive friction along the shear displacement in incremental formulation follows the relationship:

$$\Delta\mu_S^p = -\Delta\mu_{vel} \cdot \frac{\Delta u_s^p}{L1} \qquad (5\text{-}11)$$

where the increment of plastic shear displacement is defined by:

$$\Delta u_s^p = (1 - F) \cdot \Delta u_s \qquad (5\text{-}12)$$

The shear parameter L1 determines the steepness of the shear stress drop in the post-failure region. With increasing shear displacement the peak shear strength will be passed, furthermore, the upslide angle i_0 is lowered to reproduce the abrasion process resulting in a reduction of the unevenness between the joint faces and, additionally, mylonitization.

The difference between the present shear strain and the shear strain to reach the residual shear strength plateau of smoothed shear planes by abrasion is described by the parameter L2. For the reduction of the upslide angle in incremental form applies:

$$\Delta i = -i_0 \cdot \frac{\Delta u_s^p}{L2} \tag{5-13}$$

The incremental equations correspond to an exponential reduction of the adhesive friction component and the upslide angle during proceeding shear displacements on the bedding or contact plane in the post-failure state.

The effective dilatancy angle i is calculated as follows:

$$i = \arctan\frac{\tau}{\sigma_N} - \arctan\mu_K \tag{5-14}$$

Finally, the residual strength is:

$$\tau_R = \tan(\varphi_R) \cdot \sigma_N \tag{5-15}$$

and the maximum shear strength τ_{MAX} can be expressed with:

$$\tau_{MAX} = \tan\left(\varphi_R + i_0 \cdot e^{\left(-K2\frac{\sigma_N}{\sigma_K}\right)}\right) \cdot \left(1 + \Delta\mu \cdot e^{\left(-K1\frac{\sigma_N}{\sigma K}\right)}\right) \cdot \sigma_N + c \tag{5-16}$$

of dry conditions and short healing periods are similar to those of wet conditions.

5.3 Application to the Minkley-shear model and recalculation

The parameters as required for the shear model are summarised in Table 5-1. The given value have been determined in several direct shear tests which were carried out on contact planes between two bricks of precompacted crushed rock salt (Figure 5-2).

Additionally, a single shear test was recalculated to show the application of the shear parameters to the new shear model. Figure 5-3 presents the time-dependent progress of a single shear test as a stress vs. displacement diagram. The red dots represent the measured

values while the blue line describes the recalculation using the shear model parameters given in Table 5-1.

The test was realised under dry conditions without any wetting. After a 16-hour healing period applying a normal load of 10 MPa the specimen has been deformed by a constant displacement rate (0.002 mm/s) while the normal load σ_N was 1 MPa.

Table 5-1:Shear model parameters for a single shear test on the contact between two bricks of crushed rock salt (shearing after 16 hours of healing; healing under dry conditions).

parameter	symbol	value	unit
residual friction angle	ϕ_R	11	deg
upslide angle	i_0	9	deg
compressive strength contact area	σ_K	10	MPa
curvature parameter 1	K1	1.0	
curvature parameter 2	K2	1.5	
cohesion	c	0.25	MPa
maximum adhesive friction coefficient	$\Delta\mu_{MAX}$	2.6	
softening distance 1	L1	0.0003	m
softening distance 2	L2	0.015	m
distance parameter	r	0.08	
velocity factor	b_S	1.2	
critical shear velocity	v_K	0.00001	mm/s
shear stiffness	k_S	10.5	GPa/m
normal stiffness	k_N	10	GPa/m

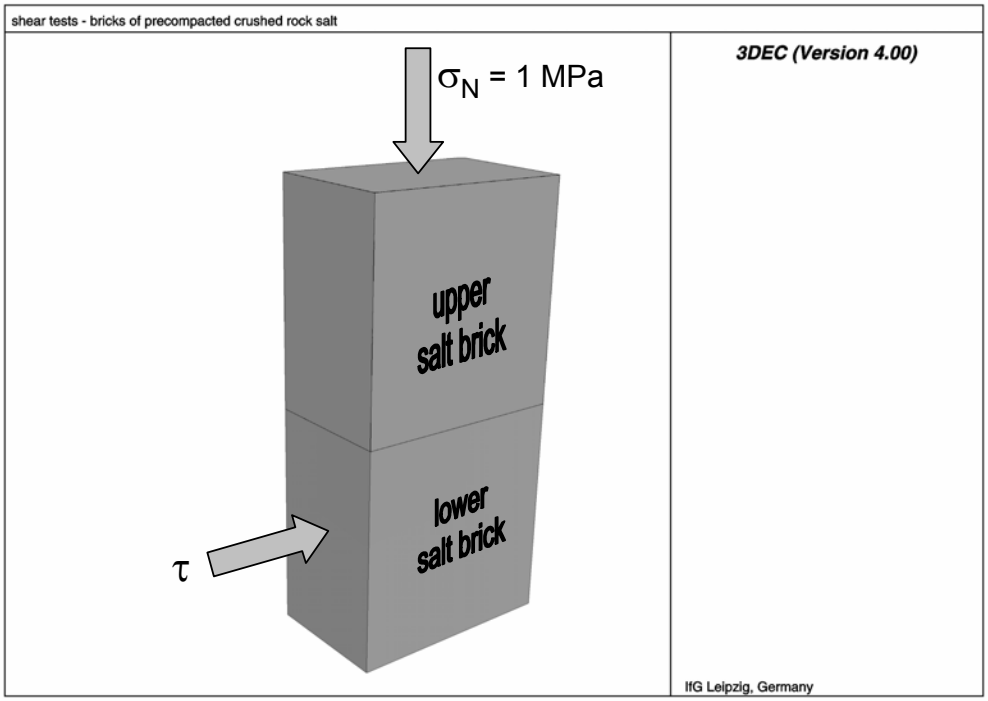

Figure 5-2: *3DEC*-simulation of shear tests on the contact plane between two bricks of pre-compacted crushed rock salt.

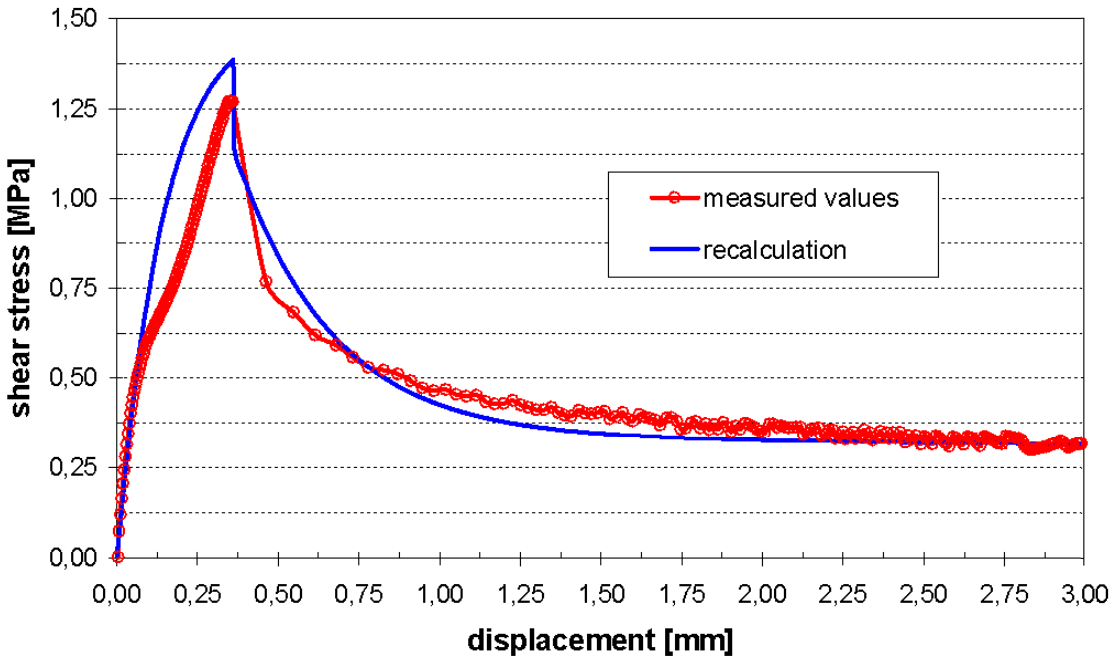

Figure 5-3: Laboratory test result to determine the peak and residual shear strengths of the contact between two bricks of crushed rock salt under dry conditions and after a period of healing of 16 hours. The red dots on the red line depict the measured values of this single shear test while the blue line describes the recalculation by *3DEC*-simulation of this test using the parameters given in Table 5-1.

6 Summary and conclusion

Our investigations on artificial saltbricks cover a wide field of relevant rock-mechanical and hydraulical properties.

Remarkably, the load bearing capacity and dilatancy behavior of the saltbricks ('dry' state) differ significantly from the behavior of the compact natural rock salt due to reachable larger deformations and relatively high load bearing capacities whereby local dilatancy is overlapped by the decrease of porosity during loading. Creep tests clearly show the faster creep of crushed salt in the range of small σ_{diff} < 15 MPa than natural rock salt.

However, it is important to note that the strength of the salt bricks is significantly reduced when moisture is present. Hydrostatic compaction experiments clearly demonstrate that besides the loading conditions the water content is the key factor for the compaction processes. After one year only in the wet samples a final porosity in the order of 2% was reached. The efficiency of the compaction depends on the stress but in each case the compaction rates are decreasing when a saturation state at around 4% remaining porosity is passed.

During the stress induced compaction permeability decreases whereby the observed permeability-porosity relationship fits very well in the generally observed variation field for the compaction of granular salt. Importantly, if water is present at the grain boundaries two-phase flow will occur associated with capillary effects. Threshold pressures determined for wet salt brick are slightly higher than the relationship estimated by Davies (1991), which may be due to the not sufficient test duration resulting in an overestimation of the threshold pressure. However taking the overall data scatter in the literature into account it can be argued that due to the difficulties of gas threshold measurements associated with lithological rock differences a unique relationship for describing capillary pressure effects seems not to be realistic.

Shear tests were performed to investigate contact properties between saltbrick surfaces and the rock salt. Whereas at dry conditions only some friction occurs, significant strengthening is observed when moisture is present because of activation of cohesion. This is in agreement with previous data reported for simulated faults in salt (Bos et al. 2000) and offers a direct proof of healing in salt rocks.

Four published constitutive models (ITASCA, HEIN, ZANG and SPIERS) describing crushed salt behaviour have been evaluated and adapted to recalculate the measured long-term hydrostatic creep behaviour.

Actually the ZHANG model (Zhang et al., 1993) seems to be the most suitable constitutive law to describe the compaction behaviour of the pre-compacted crushed-salt bricks. However an implementation in commercial available codes is necessary allowing prognosis calculations for real underground situations. Nevertheless, the potential of the SPIERS mechanism based pressure solution-model (e.g. Spiers et al., 1989) for future modeling is obvious but requires more experimental work.

The new Minkley-shear model for contact interfaces, which implies the displacement-dependent and the velocity-dependent strength softening is a suitable constitutive law to describe the contact between pre-compacted crushed salt bricks and to the host rock. This shear model is already implemented in a commercial code allowing prognosis calculation for real underground situations. The remaining task is to study and to describe the coupled HM-behaviour of such contact interfaces

Summarizing our investigations we can conclude that a reliable data base for the description of mechanical and hydraulical properties has been obtained during the course of the project. The data illustrate the excellent properties of pre-compacted crushed salt block for backfilling purposes. In this context it has to be mentioned that already practical experiences at relevant in-situ scales are available:

(1) *The "Asse-Damm"- project*
In the early 90's, a complex drift sealing project has been planned by the GSF Braunschweig comprising various components, e.g. sealing elements of concrete plugs and asphalt reservoirs as primary tight elements and secondly a masonry of pre-compacted salt bricks as long term tight element (Stockmann et al., 1991; Fig. 1-1).

(2) *The dam - project "Sondershausen"*
Focusing on a safety closure design for conventional purposes (sealing of chemical-toxic waste repositories) a multi-component drift barrier system has been developed in a german research project between 1997 and 2002 funded by BMBF[2] and TMLNU[3]. The project aims at realizing a dam concept that fulfill the long-term

[2] Bundesministerium für Bildung und Forschung

[3] Thüringer Ministerium für Landwirtschaft, Naturschutz und Umwelt

performance requirements in comparison to natural analogues (for details see Sitz et al., 2001). The sealing elements were made with artificial bricks on sand clay-bentonite basis. A static abutment was constructed as a salt brick masonry in a prismatoid shaped extension of the drift. The complete system was installed and tested in the salt mine Sondershausen. Afterwards the dam was rebuild.

However, despite the obvious improvements in knowledge and experimental data base it came out during the work that some principal challenges in relation to the salt backfill materials still remain, i.e.

(1) Understanding of physical processes which control the efficiency of granular salt compaction especially with respect to humidity effects.

(2) Development of generally agreed constitutive models for compaction in granular salt that can be reliably extrapolated to in-situ conditions.

Literature

Bechthold, W., Rothfuchs, T, Poley, A., Ghoreychi, M., Heusermann, S., Gens, A. & Olivella, S. (1999): "Backfilling and Sealing of Underground Repositories for Radioactive Waste in Salt, (BAMBUS Project)", EUR 19124 EN, CEC.

Bechthold, W., Smailos, E., Heusermann, S., Bollingerfehr, W., Bazargan Sabet, B., Rothfuchs, T., Kamlot, P., Grupa, J. Olivella & Hansen, F.D. (2004): Backfilling and Sealing of Underground Repositories for Radioactive Waste in Salt (BAMBUS-II Project), EUR 20621 EN, CEC.

Blümel, M. (2000): Improved procedures for laboratory rock test-ing. Proc. ISRM Symposium EUROCK 2000, Aachen, 573-578.

Bos, B., Peach, C.J. & Spiers, C.J. (2000): Slip behavior of simu-lated, gouge-bearing faults under conditions favouring pres-sure solution, Journal of Geophysical Research 105, 16699-16717.

CALLAHAN, G. D. & DEVRIES, K. L., (1991): Analysis of Backfilled Transuranic Waste Storage Rooms, RE/SPEC, Inc., report to Sandia National Laboratories SAND91-7052, Sandia National Laboratories,Albuquerque,NM..

CALLAHAN, G.D., LOKEN, M.C., VAN, SAMBEEK, L.L., CHEN, R., PFEIFLE, T.W., NIELAND, J.D., & HANSEN, F.D., (1995): Evaluation of Potential Crushed-Salt Constitutive Models. Sandia report, SAND95-2143, Sandia National Laboratories,Albuquerque,NM..

Callahan, G.D. Loken, M.C. Mellegard, K.D., Hansen, F.D., (1998): Crushed-salt constitutive model update. Sandia report, SAND--97-2601.

CUNDALL, P.A. & LEMOS, J.V. (1990): Numerical simulation of fault instabilities with a continuously-yield joint model. In C. Fairhurst (ed.), Proc. 2nd Int. Symp. on Rockbursts and Seismicity in Mines, Minneapolis, 8-10 June 1990: 147-152. Rotterdam: Balkema.

Davies, P.B. (1991): Evaluation of the role of threshold pressure in controlling flow of waste-generated gas into bedded salt at the Waste Isolation Pilot Plant (WIPP). Sandia Rep. SAND 90-3246.

DE MEER, S., SPIERS, C. J., PEACH, C. J., & WATANABE, T. (2002): Diffusive properties of fluid-filled grain boundaries measured electrically during active pressure solution. Earth and Planetary Science Letters, 200, 147-157.

Kazan, Y & Ghoreychi, M. (1996) : Essais In Situ CPPS – Etude Thermomécanique du Champ Proche d'un Puits de Stockage de Déchets Radioactifs dans le Sel, Rapport de la Commission Européenne EUR 16946 Fr, CEC.

HEIN, H.-J. (1991): Ein Stoffgesetz zur Beschreibung des thermomechanischen Verhaltens von Salzgranulat. Diss, RWTH Aachen.

Hildenbrand, A. (2003): Fluid Transport Process in Mudstones. PhD TH Aachen, ISBN: 3-86130-087-7.

Holcomb, D.J. & Zeuch, D.H. (1988): Consolidation of Crushed Rock Salt, Part I: EXperimental Results for Dry Salt Analyzed Using a Hot-Pressing Model, SAND88-1469, Sandia National Laboratories,Albuquerque,NM.

Hunsche, U. & Schulze, O. (1994): Das Kriechverhalten von Steinsalz.- Kali und Steinsalz, 11 (8/9), 238-255.

IFG (2005): with contributions of: BÖHNEL, H., BRÜCKNER, D., NAUMANN, D., POPP, T., SALZER, K. Investigation of the Mechanical Behaviour of Precompacted Crushed Salt in Contact to the Host Rock. NF-PRO RTDC3. WP 3.5 (Crushed Salt Engineered Barrier Behaviour). Institut für Gebirgsmechanik GmbH, Leipzig, 3 January, 2005.

(D3.5.3) Interims Report 1. Triaxial compression and permeability tests at different confining pressures on highly pre-compacted crushed salt samples including brine injection.

(D3.5.4) Interims Report 2. Shear-tests at increasing normal pressures between highly pre-compacted crushed salt blocks including brine injection and shear-test at increasing normal pressures between highly pre-compacted crushed salt blocks and host rock (rock salt) including brine injection.

IFG (2005a): Prognose der dynamischen Langzeitstabilität von Grubengebäuden im Salinar unter Berücksichtigung von Diskontinuitäts- und Schichtflächen. Final report for Forschungszentrum Karlsruhe, FKZ 02C0892. Institut für Gebirgsmechanik GmbH, Leipzig, 30 July, 2005.

IFG (2006): with contributions of: POPP, T., BÖHNEL, H., SALZER, K. (2006): Investigation of the Mechanical Behaviour of Precompacted Crushed Salt in Contact to the Host Rock. NF-PRO RTDC3. WP 3.5 (Crushed Salt Engineered Barrier Behaviour). Institut für Gebirgsmechanik GmbH, Leipzig, 2 February, 2006.

(D3.5.5) Interims Report 3. Report on long-term creep tests and gas injection tests on moistened salt bricks during compaction.

IFG (2007): with contributions of: SALZER, K., POPP, T., BÖHNEL, H. (2007): Investigation of the Mechanical Behaviour of Precompacted Crushed Salt in Contact to the Host Rock. NF-PRO RTDC3. WP 3.5 (Crushed Salt Engineered Barrier Behaviour). Institut für Gebirgsmechanik GmbH, Leipzig, 28 February, 2007.

(D3.5.6) Interims Report 4. Report on adaptation of material laws to laboratory results.

IFG (2007a): with contributions of: SALZER, K., NAUMANN, D., MÜHLBAUER, J. (2007): Investigation of the Mechanical Behaviour of Precompacted Crushed Salt in Contact to the Host Rock. NF-PRO RTDC3. WP 3.5 (Crushed Salt Engineered Barrier Behaviour). Institut für Gebirgsmechanik GmbH, Leipzig, 15 May, 2007.

(D3.5.6a) Interims Report 4. Report on adaptation of material laws to laboratory results – shear tests and shear model.

ITASCA (1995): "FLAC User's Manual," Itasca Consulting Group, Inc., Minneapolis, Minnesota.

ITASCA (2005): FLAC^{3D} – Fast Lagrangian Analysis of Continua in 3 Dimensions, Version 3.0, User's Manual. ITASCA Consulting Group, Inc. Minneapolis, Minnesota, USA

Korthaus, E. (1996): 'Consolidation and Deviatoric Deformation Behaviour of Dry Crushed Salt", Proc. of 4th Conf. on the Mechanical Behavior of Salt, Montreal, Canada, 365-377, 1996.

Lerch, C. (1999): Abschlussbericht zum Projekt BAMBUS. Teilprojekt Comparative Study on Crushed Salt (CS). Deutsche Gesellschaft zum Bau und Betrieb von Endlagern für Abfallstoffe mbH (DBE), PEINE.

Liedtke, L. Kojic, M., Dvorkin, E.N.& K.J.Bathe (1986): A pressure sensitive creep model for crushed rock salt", Proceedings Conf. Numerical Methods in Geomechanics, Stuttgart September 16-18, 1 -19.

Marschall, P., Horseman, S. & Gimmi, T. (2005): Characterisation of Gas Transport Properties of the Opalinus Clay, a Potential Host Rock Formation for Radioactive Waste Disposal. Oil & Gas Science and Technology – Rev. IFP, Vol. 60, No. 1, pp. 121 - 139.

Müller-Lyda, I. (1999): Permeabilität von aufgelockertem Steinsalz. Ableitung einer Permeabilitäts-Druck-Relation für Langzeitsicherheitsanalysen, GRS-151, Braunschweig.

NEA-EC 2003. Engineered Barrier Systems and the Safety of Deep Geological Repositories, State-of-the-art Report, EUR 19964 EN. CEC.

Olivella S., A. Pudewills, A. Gens, U. Heemann (2001): Review of TSDE In Situ Test Thermo-Mechanical Modelling. CLUSTER Seminar, organised by CEE, Mol, EUR 19954, pp 103-118.

Popp, T., Kern, H. & Schulze O. (2001): The evolution of dilatancy and permeability in rock salt during hydrostatic com-paction and triaxial deformation.- J. Geophys. Res. 106, No. B3, 4061-4078.

Popp, T., Wiedemann, M., Kansy, A. & Pusch, G. (2007): Gas transport in dry rock salt – implications from laboratory investigations and field studies. In: Wallner, M., Lux, K.H., Minkley, W. & Hardy, H. R. The Mechanical Behavior of Salt – Understanding of THMC Processes in Salt: 6th Conference (SaltMech6), Hannover, Germany, 22–25 May 2007. Publ.: Taylor and Francis, ISBN: 9780415443982, 17 – 26.

Sitz, P.; Koch, G.; Gruner, M. (2001). Langzeitstabile Streckenverschlussbauwerke im Salinar. Wissenschaftliche Berichte FZKA - PTE, Nr. 7, Juli 2001, 393 – 436.

Sjaardema, G. D., & Krieg, R. D. (1987): A Constitutive Model for the Consolidation of WIPP Crushed Salt and Its Use in Analyses of Backfilles Shaft and Drift Configurations, Sandia National Laboratories, SAND87-1977, Sandia National Laboratories, Albuquerque, NM.

Spiers, C. J., Peach, C. J., Brzesowsky, R. H., Schutjens, P. M. T. M., Liezenberg, J. L., Zwart, H.J. (1989): Long-term rheological and transport properties of dry and wet salt rocks, Nuclear Science and Technology, EUR 11848 EN, Office for Official Publications of the European Communities, Luxembourg. 1989.

Spiers, C.J. & Carter, N.L. (1998): Microphysics of rocksalt flow in nature. In: M. Aubertin (Ed.), The Mechanical Behavior of Salt: Proceedings of the Fourth Conference. Trans. Tech. Publ. Series on Rock and Soil Mechanics, 22, 115-128.

Spiers, C. J.; Grupa, J.; Popp, T.; Salzer, K.; Stührenberg, D.; Zang, X. (2005): Buffer/Backfill in Salt: Long-term compaction, effect of additives and behaviour of pre-compacted bricks. NF-PRO Second Training Course and Workshop, Cardiff, 19.-20.10.2005.

Stockmann, N. (1994): Dammbau im Salzgebirge. Abschlußbericht Projektphase II, GSF-Bericht 18/94, Kap. 8.1.4, 243 ff

Stormont, J.C. & Daemen, J.J.K. (1992): Laboratory study of gas permeability changes in rock salt during deformation, Int. J. Rock Mech. Min. Sci. Geomech. Abstr., 29, 325-342.

Washburn, E.W. (1921): Note on a method of determining the distribution of pore sizes in a porous material, Proceedings of the National Acadamy of Science, 115-116. Bulletin, 63, 723-760.

Zhang, C. L., Heemann, U., Schmidt, M. W., Staupendahl, G. (1993): Constitutive model for description of compaction behaviour of crushed salt backfill. Proc. ISRM International Symposium, EUROCK 93, Lisbon

Zhang, C. L., Schmidt, M. W., Staupendahl, G., Heemann, U. (1993): Entwicklung eines Stoffansatzes zur Beschreibung des Kompaktionsverhaltens von Salzgrus. Bericht Nr. 93-73 aus dem Institut für Statik der Technischen Universität Braunschweig

Zhang, X.; Grupa, J. (2004): Porosity/permeability reduction in crushed rocksalt: An overview of the literature, NRG & UU Internal Report.

Zhang, X.; Grupa, J. (2006): Compaction behaviour and permeability of low porosity compacted salt grit (dry and wet) – Experimental Investigation and Microphysical Modelling. NF-PRO RTDC3. WP 3.5 (Crushed Salt Engineered Barrier Behaviour **D3.5.1**). Utrecht University and NRG, 16 August, 2006. Marschall, P., Horseman, S. & Gimmi, T. 2005. Characterisation of Gas Transport Properties of the Opalinus Clay, a Potential Host Rock Formation for Radioactive Waste Disposal. Oil & Gas Science and Technology – Rev. IFP, Vol. 60, No. 1, 121-139.